Met Office

Forecasting Research Technical Report: The 5A Orographic Drag Scheme: Design and Testing

December 2010

Helen Wells

1 Summary

This report describes a new orographic drag parametrization in the MetUM and assesses the performance of the new scheme compared to the current scheme ([Webster et al., 2003]) through testing using a global numerical weather prediction (NWP) configuration at N320L70 resolution.

The new parametrization is based on the [Lott and Miller, 1997] scheme, currently operational at ECMWF and other operational centres, but with the following modifications:

- A different averaging depth is used to calculate the parametrized low-level Froude number and depth of flow blocking region.
- An option has been introduced to smooth the gravity wave drag over a vertical hydrostatic wavelength.
- An initial attempt has been made to represent the effects of non-hydrostatic waves.

The formulation of the new parametrization is believed to be an improvement on the current parametrization since:

- The flow blocking part of the parametrization has a better physical basis than that used in [Webster et al., 2003] (where the flow blocking drag calculation is based on linear gravity wave theory).
- The scheme is more flexible than the current scheme allowing separate specification of the amplitude of the flow blocking response and the gravity wave response.
- It is hoped that the option to smooth the gravity wave drag will reduce numerical stability problems associated with large accelerations being applied over single model levels.

The headline results in this report are:

- The performance of the new parametrization is broadly neutral when compared to the current scheme. However, the new scheme does slightly degrade the tropical 850 hPa winds, compared against the analysis. If a forthcoming VAR trial indicates that this result is robust then some further tuning will be required before the parametrization could become operational.
- Smoothing the drag over a vertical wavelength appears to be a viable option since it does not degrade any model fields and it allows the amplitude of the gravity waves launched to be increased without significantly increasing the drag in the upper stratosphere.
- Even when smoothing is applied it is not possible to allow orographic gravity wave drag to be applied above a height of 40 km since it leads to very large changes in the zonal flow (of over 100 ms^{-1}). These large changes in the zonal flow are indicative of the potential for model stability problems (which the current parametrization also displays).

- As yet it has not been possible to find a competitive configuration of the new parametrization with a reduced critical Froude number compared to the current operational value of 4. This is disappointing since it is believed that this setting is unphysical although it is suggested in this report that this large critical Froude number may be required in order to account for variability in low-level Froude number in a grid box (arising from effects such as variable low-level flow and stability or decoupled flow in valleys). Further work is required to assess this possibility.
- Initial results indicate that it may be possible to find a competitive configuration of the new parametrization which does not use the current slope ancillary fields. This change could be beneficial as these fields do not converge at high resolution and appear noisy.
- The non-hydrostatic formulation requires further thought, since currently it only has a significant effect on the vertical distribution of gravity wave drag when all gravity waves are assumed to propagate at an angle of around 45°.

2 Introduction

The current orographic drag scheme, known as the 4a scheme, in the Met Office Unified Model (hereafter the MetUM) has been operational since 2002 and is documented in [Webster et al., 2003] (hereafter, W03). The 4a scheme parametrizes the drag associated with low-level flow blocking by sub-grid scale orography (SSO) and breaking gravity waves forced by the SSO. In the 4a scheme the linear gravity wave stress is calculated and then partitioned into flow blocking stress and gravity wave stress based on the low-level Froude number, $F = U/NH$ (where U is the wind-speed, N is the buoyancy frequency and H is the height of the SSO). If F is greater than the critical Froude number, F_c, then the all of the flow is assumed to pass over the SSO and all of the stress is launched as gravity waves. The gravity-wave propagation aspects of the scheme are based on the ideas of [McFarlane, 1987]. At every level the scheme tests to see if the amplitude of the parametrized wave exceeds a critical amplitude (the largest wave amplitude which can be supported by that layer of flow), if this critical amplitude is exceeded then a proportion of the stress carried by the wave is deposited as drag at that level and then the wave continues to propagate upwards carrying a reduced stress. Conversely if F is less than the critical Froude number, F_c, then the scheme applies blocked flow drag between the surface and the mountain top, and the launch stress of the gravity waves is reduced accordingly.

In recent years we have been working on designing a replacement for the 4a scheme in order to address the following significant deficiencies:

1. The physical basis of the flow blocking stress calculation in the 4a scheme is relatively weak. Given that flow blocking drag occurs through a very different physical mechanism to gravity wave drag it is inappropriate to calculate it using equations based on gravity wave theory. The new scheme therefore has a more physically appropriate basis for the flow blocking calculations, based on bluff body dynamics. Additionally the formulation of the flow blocking drag calculation means that it will not reverse the low-level flow (which is an undesirable feature of the 4a scheme).

2. The 4a scheme has only a single coefficient to determine the amplitude of the stress response, a parameter called the inverse wavenumber constant, $\hat{K}^{-1}$. This limits the flexibility of the scheme since it means that one cannot adjust the magnitude of the flow blocking stress independently of the gravity wave stress. We also believe that this feature has led to an unphysical optimal setting of F_c in the 4a scheme ($F_c = 4$ when current theoretical and experimental results constrain it to lie in the range $[0.7, 1]$). The new scheme therefore has two separate coefficients to determine the magnitude of the flow blocking stress and gravity wave stress.

3. We believe that (compared with reality) the gravity waves have been tuned down in the 4a scheme in order to prevent numerical stability problems associated with large accelerations

being deposited at single grid points in the stratosphere. Therefore we have designed the new scheme to include some features which we hope will allow us to launch larger amplitude waves without degrading model performance in the stratosphere, these features include smoothing any parametrized drag over a vertical wavelength of a hydrostatic gravity wave and an initial attempt to represent the effect of waves propagating horizontally out of the grid column.

The layout of this report is as follows. The next section gives a detailed description of the new scheme. Section 4 and section 5 detail the results from testing the new scheme in the NWP (numerical weather prediction) model using a single forecast and a case study suite respectively. Section 6 details the current optimal set-up for the new scheme (based on the testing results) and highlights the strengths and weaknesses of the scheme. Section 7 presents a summary of the report.

3 Description of the new orographic drag parametrization

The new scheme, known as the 5a scheme, is essentially a variant of the [Lott and Miller, 1997] (hereafter, LM97) scheme, currently operational at ECMWF and various other operational centres. We have added some new features to the scheme namely: a different calculation to determine the low-level Froude number; an option to smooth all gravity wave drag over a vertical wavelength and an initial (very basic) attempt to represent the effect of waves propagating horizontally out of the grid column. The scheme is available for general use in the MetUM from vn7.8 and may be controlled from the Unified Model User Interface (UMUI). Technical documentation to accompany the code is available from my internal webpage. In this section we shall describe the new scheme, contrasting it with the 4a scheme as appropriate.

3.1 Characterisation of sub-grid scale orography

The new scheme retains the SSO parameters used by the 4a scheme namely:

- The standard deviation of the SSO from the grid-box mean, σ,
- The squared grid-box average gradient in the x direction, $\sigma_{xx} = \overline{\frac{\partial h}{\partial x}^2}$,
- The squared grid-box average gradient in the xy direction, $\sigma_{xy} = \overline{\frac{\partial h}{\partial x}\frac{\partial h}{\partial y}}$,
- The squared grid-box average gradient in the y direction, $\sigma_{yy} = \overline{\frac{\partial h}{\partial y}^2}$,

where $h(x, y)$ is the SSO topography and the over-bar denotes the average over the grid-box. Despite using the same basic parameters the new scheme uses a different conceptual model regarding the underlying topography so that it is based on LM97 rather than [Gregory et al., 1998] (hereafter, GSM98). The SSO parameters of LM97 are used since this allows us to use unmodified versions of their flow blocking and gravity wave schemes.

The 4a scheme is based upon the ideas of GSM98 which assumes a statistical spectral representation of the orography such that the amplitude of the orographic spectrum, A(k), fits a power law of the form ck^d where c and d are constants. The constant d was estimated from average values of 1-D spectra computed for North Wales, West Colorado and the Appalachians and assuming isotropy. In contrast, LM97 arbitrarily assume that the orography is made up of uniformly distributed elliptical mountains (based on the same orographic statistics as GSM98, albeit in different combinations). The geometry of the mountain can be written in the form

$$h(x,y) = \frac{H}{1 + x'^2/a^2 + y'^2/b^2}, \tag{1}$$

where a and b are such that $\gamma = a/b \leq 1$.

Following LM97 we compute four SSO parameters:

1. The standard deviation of the SSO from the grid-box mean, σ, from which the sub-grid scale mountain height is calculated as $H = n_\sigma \sigma$, where n_σ is a tuning constant (set to 2.5 by default).
2. The anisotropy of the SSO, γ, where $\gamma^2 = \frac{\sigma_{xx}+\sigma_{yy}-\sqrt{\left((\sigma_{xx}-\sigma_{yy})^2+4\sigma_{xy}^2\right)}}{\sigma_{xx}+\sigma_{yy}+\sqrt{\left((\sigma_{xx}-\sigma_{yy})^2+4\sigma_{xy}^2\right)}}$.
3. The angle between the low-level wind and the major axis of the topography, Ψ, where $\tan 2\Psi = \frac{2\sigma_{xy}}{\sigma_{xx}-\sigma_{yy}}$
4. The mean slope of the SSO (along the major axis), α, where $\alpha^2 = 0.5\left(\sigma_{xx} + \sigma_{yy} + \sqrt{\left[(\sigma_{xx}-\sigma_{yy})^2 + 4\sigma_{xy}^2\right]}\right)$
   Note that, in contrast to LM97, we have defined the slope as a non-dimensional number (α) rather than as an angle ($\arctan\alpha$) as it is used as a non-dimensional number in all calculations in LM97.

For more information on the derivation of these parameters see the Appendix of LM97.

3.2 Flow Blocking

The treatment of flow blocking in the new scheme is based on LM97 where the drag exerted on a mountain as a result of flow splitting and wake formation is given by

$$D_b(z) = -\rho_s C_d l(z) \frac{\mathbf{U}|\mathbf{U}|}{2}, \tag{2}$$

where $l(z)$ is the horizontal width of the mountain at a height, z, and C_d is a constant of order unity. The full drag expression for flow blocking is

$$D_b(z) = -C_d \max\left(2 - \frac{1}{r}, 0\right) \rho \frac{\alpha}{2\sigma} \left(\frac{Z_b - z}{z + \sigma}\right)^{1/2} (B\cos^2\Psi + C\sin^2\Psi) \frac{\mathbf{U}|\mathbf{U}|}{2}, \tag{3}$$

where $B = 1 - 0.18\gamma - 0.04\gamma^2$ and $C = 0.48\gamma + 0.3\gamma^2$ and r is the aspect ratio of the obstacle as seen by the incident flow

$$r = \left(\frac{\cos^2 \Psi + \gamma^2 \sin^2 \Psi}{\gamma^2 \cos^2 \Psi + \sin^2 \Psi} \right)^{1/2}, \tag{4}$$

so that the drag coefficient, C_d, is multiplied by a number between 1 and 2 depending on whether the flow is normal to or parallel to the major axis of the orography. Note that the expression for r differs from the formula in LM97 as the LM97 derivation is incorrect (Ayrton Zadra, personal communication). Following LM97, a quasi-implicit formulation for numerical stability has been adopted in which $|\mathbf{U}|$ is taken at time$= t$ and $\mathbf{U}$ at time$= t + \Delta t$.

Following the results of [Vosper et al., 2009], who showed that the stability above a mountain can have a significant effect on the flow blocking drag, we define the depth of the blocked layer to be

$$Z_b = \max(0, H(1 - F_{av}/F_c)), \tag{5}$$

where F_c is the critical Froude number. Here, we introduce the quantity

$$F_{av} = \bar{U}/N_{av}H \tag{6}$$

which is the Froude number calculated for U and N averaged over a depth Z_{av} defined as

$$Z_{av} = \max(H, Z_n) + \bar{U}/N_{av}, \tag{7}$$

where Z_n is the depth of a near-surface neutral layer (if present), $\bar{U}$ has been depth-averaged from the surface to $z = Z_{av}$ and N_{av} is a bulk average value of N over the same depth i.e.

$$N_{av} = \sqrt{\left(\frac{g}{\theta_0} \frac{\theta_{av} - \theta_0}{Z_{av}} \right)}, \tag{8}$$

where θ_0 and θ_{av} are the potential temperatures at the surface and $z = Z_{av}$ respectively. Note that the wind speed, $\bar{U}$, is currently resolved in the direction of the low-level flow (u_{low} and v_{low} defined in section 3.3), further work is required to determine whether this is the best choice. Since the inputs required to solve Eq. 7 for Z_{av} are themselves averaged from the surface to Z_{av} this equation must be solved iteratively.

3.3 Gravity waves

The treatment of hydrostatic gravity waves is based on the LM97 scheme which uses the analytical expression for the drag due to uniformly distributed elliptical mountains derived by [Phillips, 1984]. For a single elliptical mountain the mountain wave stress is

$$(\tau_{\parallel}, \tau_{\perp}) = \rho_s U_s N_s H^2 b G (B \cos^2 \Psi_s + C \sin^2 \Psi_s, (B - C) \sin \Psi_s \cos \Psi_s), \tag{9}$$

where

- $\tau_{\parallel}$ and $\tau_{\perp}$ are the flow parallel and flow normal stress respectively.
- ρ_s, U_s, N_s and Ψ_s are the low-level average density, wind-speed, buoyancy frequency and the angle between the low-level flow and the major axis of the orography respectively. Following LM97 these quantities will be averaged from $z = 0.5H$ to $z = H$ in order to reduce diurnal effects on the drag (in contrast to the 4a scheme where these quantities are averaged from the surface to H).
- G is a function of the mountain sharpness, here used as a constant of order unity (in fact it is a function of the exponent used in the definition of the elliptical orography, which is unity in LM97 and variable in [Scinocca and McFarlane, 2000])

If b or a is significantly less than the grid-box length Δx then there are typically $\Delta x^2/4ab$ ridges inside the grid-box. Summing the associated forces we find the stress per unit area is

$$(\tau_{\parallel}, \tau_{\perp}) = \rho_s U_s N_s (\alpha/\sigma) H^2 G(B \cos^2 \Psi_s + C \sin^2 \Psi_s, (B - C) \sin \Psi_s \cos \Psi_s), \tag{10}$$

where a has been replaced by σ/α where α is the root mean square slope in the direction of the major axis of the orography and σ is the standard deviation of the orography. Following [Brown, 2005] we modify the original LM97 formulation to represent a cut-off mountain where only the part of the mountain above the flow blocking layer contributes to the gravity wave drag so that

$$(\tau_{\parallel}, \tau_{\perp}) = \rho_s U_s N_s (\alpha/\sigma) (H_{eff}^2/4) G(B \cos^2 \Psi_s + C \sin^2 \Psi_s, (B - C) \sin \Psi_s \cos \Psi_s), \tag{11}$$

where $H_{eff} = H - Z_b$ where Z_b is the depth of the blocked layer. Note here I have assumed that depth of blocked layer is less than H, if we relax this assumption (as LM97 did) then we need to change the divisor for H_{eff}.

The gravity-wave propagation aspects of the scheme are based on the ideas of [McFarlane, 1987], with a small change intended to account for non-hydrostatic wave propagation. The waves are assumed to be steady and monochromatic, with a horizontal wave vector aligned with the depth averaged low-level horizontal wind vector, and Coriolis effects are neglected. In the absence of wave breaking, the wave stress is constant with height, while the change in wave amplitude between adjacent grid levels is given by

$$\eta = H_{eff} [(\rho_s N_s U_s)/(\rho N U)]^{0.5}, \tag{12}$$

where η is the vertical displacement associated with the gravity wave. In other words it is determined by the decay of air density with altitude (which results in a growth of wave amplitude with increasing height) and changes in both the buoyancy frequency and the background wind. Decreases in the

wind (resolved in the direction of the horizontal wave vector) will result in a growth in wave amplitude, as will decreases in the buoyancy frequency.

Diagnosis of wave breaking and the deposition of wave stress follows that described by GSM98 which is based on the saturation hypothesis of [Lindzen, 1981]. Wave breaking is assumed to take place when the local Froude number, $U/\eta N$, falls below a critical value, F_{sat}. When this occurs a proportion of the wave stress is exerted on the flow and the wave amplitude is reduced accordingly such that $U/\eta N = F_{sat}$.

If the 'Smooth' option is selected then when wave breaking is diagnosed the scheme deposits the stress over a vertical wavelength

$$\lambda z = \chi \frac{2\pi U}{N} \tag{13}$$

where U/N is constrained to lie in the range $[\lambda z_{min}, \lambda z_{max}]$, where $\lambda z_{\min}$ and $\lambda z_{\max}$ are tuning constants which prevent the wavelength becoming too small or too large (either scenario would not be beneficial for the smoothing). The tuning constant, χ, is used to define the fraction of the wavelength that drag should be deposited over (set to 1 by default).

This is beneficial for two reasons:

1. It improves the physical representation of gravity wave breaking. The idea of a vertical length scale for stress deposition comes from Fig. 12 of [Epifanio and Qian, 2008] which shows that, for an ensemble of quasi-LES (Large-Eddy Simulations) of low-level wave breaking, stress deposition occurs over a depth of between $0.5\lambda_z$ and λ_z.

2. It makes the parametrization more numerically stable by smoothing out the stress deposition.

The scheme deposits the same stress over every level from $z - 0.5\chi\lambda_z$ to $z + 0.5\chi\lambda_z$. If $z - 0.5\chi\lambda z$ extends below the mountain top then the drag is applied down to the surface so that drag is applied over the range ($z = 0, z = z + 0.5\chi\lambda z$).

To summarise the new scheme treats hydrostatic gravity waves in the following way:

- Surface stress calculation based on LM97 with the cut-off mountain correction proposed by [Brown, 2005].
- Wave propagation based on [McFarlane, 1987].
- Wave breaking is diagnosed when the local Froude number drops below a critical value. Wave breaking stress is then deposited over a vertical wavelength of the gravity wave (following the work of [Epifanio and Qian, 2008]).

3.4 Non-hydrostatic option

Due to the requirement for parametrizations to be computationally efficient, orographic gravity wave parametrizations have traditionally been column-based and thus have not allowed for the effect of non-hydrostatic wave propagation. Currently it is not considered feasible to move away from

a column-based scheme, but here we aim to account for the wave stress associated with non-hydrostatic waves propagating out of the sides of the grid-box by depositing the stress at the height where the wave exits the grid-box. The ratio of the vertical group velocity of the wave, c_{gz}, to the horizontal group velocity, c_{gk} is given by

$$\beta = c_{gz}/c_{gk} = m/k \tag{14}$$

where k and m are the horizontal and vertical wavenumbers of the gravity wave respectively. Note we have assumed that the wavenumber perpendicular to the flow (l) is zero and that the intrinsic frequency of the waves is zero. Three possible approaches for determining β are:

1. Calculate β based on the group velocity of the waves. To do this an estimate of the horizontal wavenumber, k, is required. One option is to approximate k by $1/L$ where L is the length-scale of the topography in the direction of the low-level wave stress (which can be derived from the LM97 orographic statistics). A fuller description of this calculation is given below.

2. Estimate β from a fixed shape profile. This profile might be diagnosed from high resolution forecast simulations (e.g. EC/UM Andes simulations of [Shutts and Vosper, 2011]) or calculated from idealised simulations.

3. Assume a fixed value for β.

Currently our default option is to use a fixed value for β although option 1. (dynamically adjusting β) has also been coded up.

In the absence of wave breaking, the change in stress over a model level will be given by the ratio of the flux of stress out of the sides of the grid box to the total flux out of the grid-box.

$$\tau(z) = \tau(z - \Delta z) \times \left(1 - \frac{\tau|c_{gx}|\Delta z\Delta y + \tau|c_{gy}|\Delta z\Delta x}{\tau c_{gz}\Delta x\Delta y + \tau|c_{gx}|\Delta z\Delta y + \tau|c_{gy}|\Delta z\Delta x}\right) \tag{15}$$

Substituting for $|c_{gx}| = |c_{gk}||\cos\psi|$, $|c_{gy}| = |c_{gk}||\sin\psi|$ and dividing by $|c_{gk}|$ gives:

$$\tau(z) = \tau(z - \Delta z) \times \left(1 - \frac{|\cos\psi|\Delta z\Delta y + |\sin\psi|\Delta z\Delta x}{\beta\Delta x\Delta y + |\cos\psi|\Delta z\Delta y + |\sin\psi|\Delta z\Delta x}\right) \tag{16}$$

where ψ is the angle between the low-level wind direction and the x-axis (used to calculate Ψ in LM97). For the simple case where $\Delta x = \Delta y = \Delta z$ and $\psi = 0$ this reduces to

$$\tau(z) = \tau(z - \Delta z)\left(1 - \frac{1}{\beta + 1}\right) \tag{17}$$

Therefore if at some height $\beta \to 0$ then $\tau(z) \to 0$ and all of the wave stress is assumed to advect laterally out of the grid-box and is deposited at this height by the column-based scheme. Conversely if $\beta \to \infty$ then $\tau(z) \to \tau(z - \Delta z)$ and all of the stress is assumed to propagate upwards.

For the dynamically adjusting β option, β is calculated based on the group velocity of the waves and then parametrized in terms of known variables. The vertical wavenumber can be related to the horizontal wavenumber via

$$m^2 = N^2/U^2 - k^2. \tag{18}$$

Substituting Eq. 18 into Eq. 14 (the ratio of the vertical group velocity to the horizontal group velocity) we obtain

$$\beta = (1 - k^2U^2/N^2)^{1/2}/(kU/N). \tag{19}$$

The only unknown variable in this equation is the horizontal wavenumber, k. Here I choose to relate k to the SSO parameters in LM97 by assuming $k = 1/L$ where

$$L = a\cos\xi + b\sin\xi = \sigma/\alpha\cos\xi + \sigma/\alpha\gamma\sin\xi. \tag{20}$$

and $\xi = \Psi_s + \arctan(\tau_\perp/\tau_\parallel)$ is the angle between the low-level stress vector and the major axis of the orography. Physically L is the length scale of the topography in the direction of the low-level wave stress (and hence in the direction of k). Note that a major issue with this dynamically adjusting β is that typically at N320 resolution this calculation predicts $\beta \sim O(100)$, whereas to see significant effects from the non-hydrostatic correction one requires $\beta \sim O(1)$. This issue will be discussed further in section 4.7.

4 Results from a single forecast run

Initial tests were done using for a N320L70 global model (corresponding to a grid spacing of approximately 40 km at a latitude of 40°). The model was initialised at 06 UTC on 08 December 2008 and run for 24 hours. All of the output was then averaged over this 24 hour period to give an initial insight into the behaviour of the new scheme. Note that the SSO ancillary files used for this run were filtered to remove scales shorter than 6 km. These ancillaries are the default choice at all other global model resolutions, however for performance reasons older ancillaries, filtered to remove scales shorter than 40 km, have been retained at N320 resolution.

The scheme was configured as follows for the majority of tests: $Cd = 10$, $G = 0.8$, $F_c = 4$, $F_{sat} = 1$, $Z0_{eff} = 0.45$ (effective roughness length used by the orographic form drag parametrization), gravity wave drag off above 40 km, smoothing off, non-hydrostatic option off. This 5a control set-up was chosen to give broadly comparable results to the standard set-up of the 4a scheme. The behaviour of the 5a control will be described briefly in the following subsection (and compared to the 4a scheme), while subsequent subsections document the sensitivity to changing various parameters in the 5a control.

4.1 Comparison of 5a CONTROL to 4a CONTROL

Figure 1 shows the daily averaged zonal surface stress for the 4a CONTROL and 5a CONTROL. It is clear that the surface stresses have a similar magnitude and geographical distribution in the two simulations. The zonally averaged difference in zonal surface stress between the two simulations is indicative of slightly larger surface stresses in the 5a scheme than in the 4a scheme.

The surface stress is dominated by the contribution from the flow blocking stress in both simulations with the gravity wave surface stress being approximately an order of magnitude smaller. The 5a scheme has been tuned so that most diagnostics are broadly similar. However significant differences between the two schemes are seen in two areas. First, the magnitude of the gravity wave accelerations shown in Fig 2 is much smaller in 5a CONTROL than in 4a CONTROL. It is believed that this differences are due to using a smaller value of G than is appropriate for the 5a CONTROL, and could be easily rectified. Second, the near surface flow blocking accelerations, shown in Fig. 3, are much weaker in the 5a scheme than the 4a scheme. This difference arises from a difference in the formulation of the schemes. The flow blocking accelerations at a given height in the 5a scheme are dependent on the velocity squared at that height whereas those in the 4a scheme are dependent on the depth average velocity from the surface to the mountain height. This means that the 5a scheme gives systematically smaller near surface accelerations than the 4a scheme, but that differences are minimal higher up in the atmosphere. Therefore, in order to obtain competitive performance compared to the 4a scheme, the orographic roughness length ($Z0_{eff}$) in the 5a CONTROL has been increased from 0.15m (4a CONTROL value) to 0.45m.

4.2 Tuning parameter 1: Sensitivity to Critical Froude Number, F_c

In the operational configuration of the 4a scheme the critical Froude number is set to $F_c = 4$. However numerical and laboratory experiments and linear theory of flow over hills suggest that it should take a value close to unity, implying that the current default setting is unphysical. The flow blocking acceleration in the 5a scheme is sensitive to F_c in two ways:

1. Increasing F_c increases the parametrized depth of the flow blocking layer via $Z_b = H(1 - F_{av}/F_c)$.

2. Increasing F_c increases the likelihood of flow blocking being parametrized as it determines the threshold for moving from just gravity wave drag to a combination of gravity wave and flow blocking drag.

(Note: in the 5a scheme F_c only effects the gravity wave drag via the blocked layer depth calculation (which determines the amplitude of the wave launched through the cut-off mountain approximation $H_{eff} = H - Z_b$), this effect can be balanced by changes in the gravity wave amplitude factor, G). It is possible to investigate the relative importance of these dependencies for the flow blocking drag

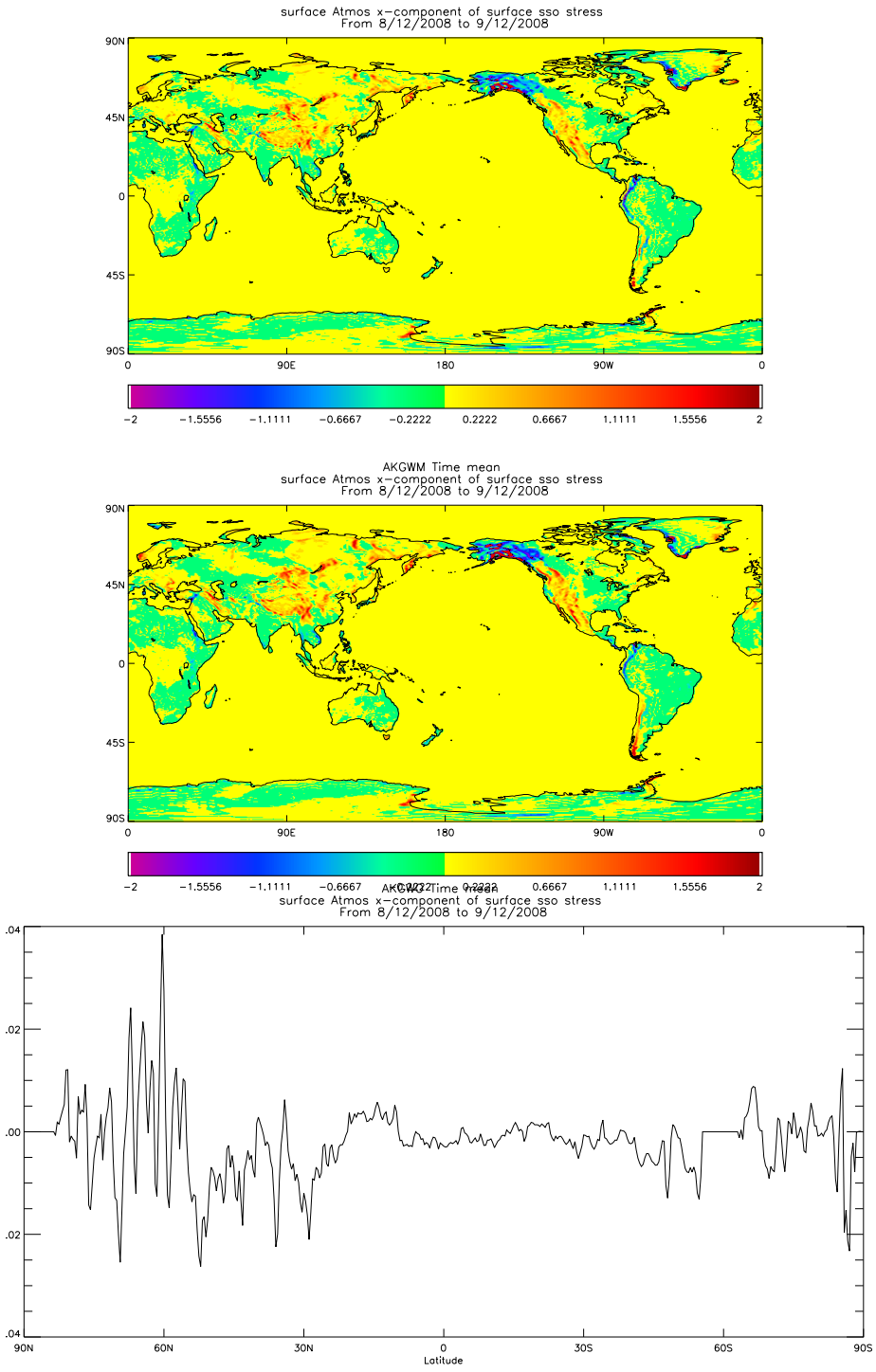

Figure 1: Daily averaged zonal surface stress (gravity wave + flow blocking) for (top) 4a CONTROL (middle) 5a CONTROL and (bottom) Zonally averaged difference between 4a CONTROL and 5a CONTROL.

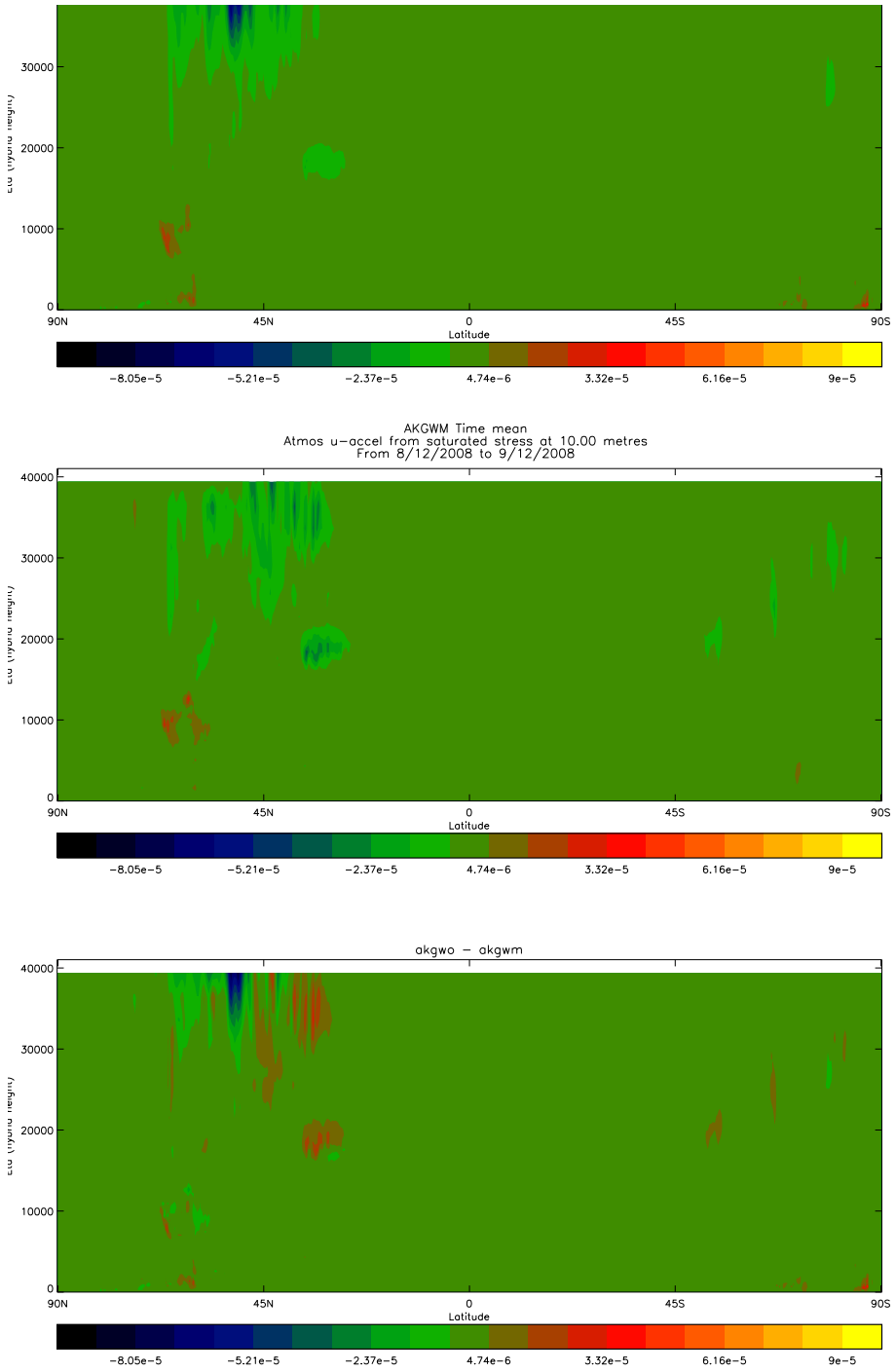

Figure 2: Daily averaged zonally averaged zonal gravity wave accelerations for (top) 4a CONTROL (middle) 5a CONTROL and (bottom) Difference between the 4a CONTROL and 5a CONTROL.

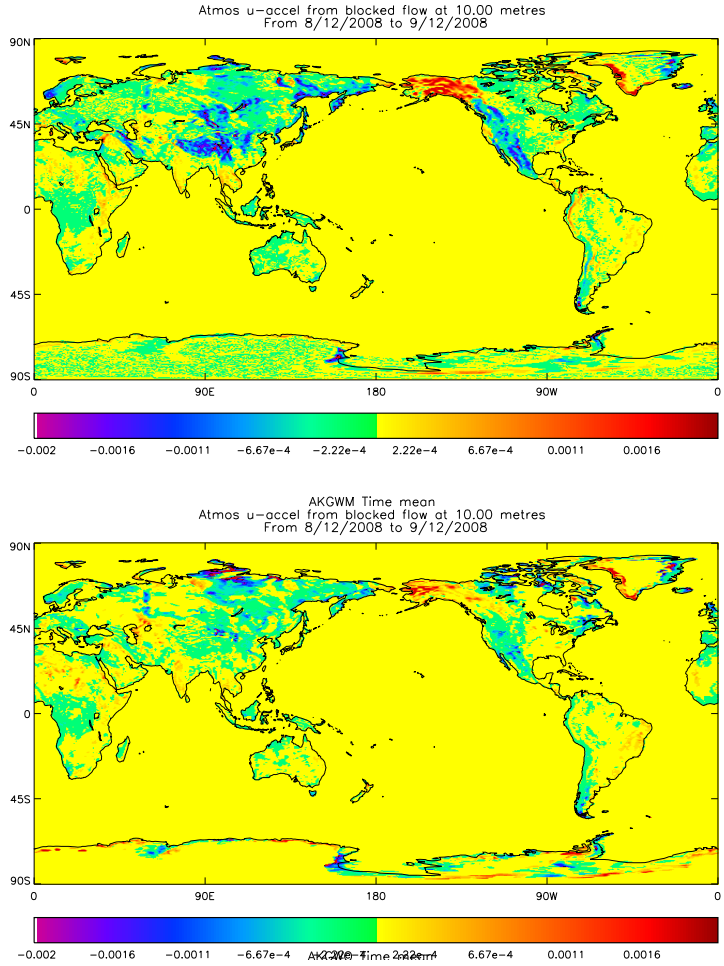

Figure 3: Daily averaged zonal flow blocking accelerations at 10m (lowest model level) for (top) 4a CONTROL (bottom) 5a CONTROL.

by modifying the code so that a different value of F_c is used to define the blocking depth than is used to define the threshold for parametrizing flow blocking drag.

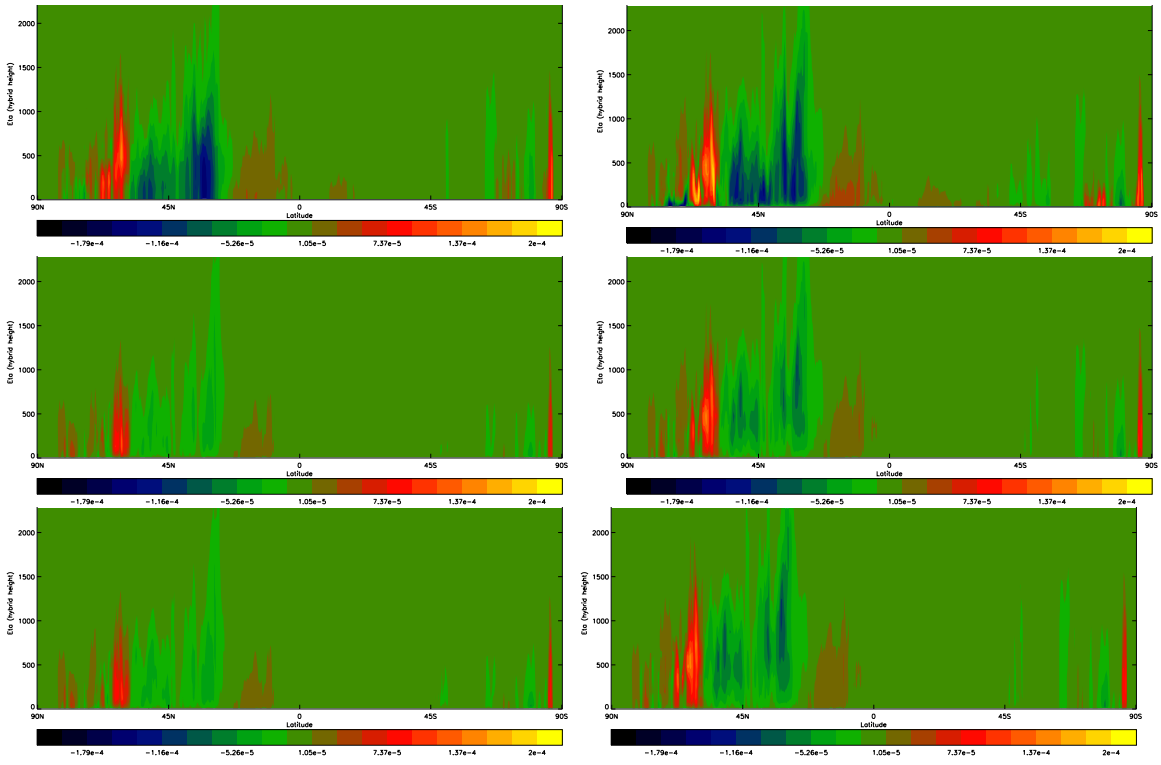

Figure 4: Zonally averaged daily averaged flow blocking accelerations for (top left) 4a CONTROL ($F_c = 4$) (top right) 5a CONTROL $F_c = 4$, (middle left) 5a scheme $F_c = 1$, (middle right) 5a scheme with threshold for flow blocking $F_c = 1$, blocking depth $F_c = 4$, (bottom left) 5a scheme with threshold for flow blocking $F_c = 4$, blocking depth $F_c = 1$ and (bottom right) 5a scheme with threshold for flow blocking $F_c = 1$, blocking depth set to mountain height ($Z_b = H$)

Comparison of simulations using the 5a scheme with $F_c = 4$ (Fig.4, top right) and $F_c = 1$ (Fig.4, middle left) reveal that the flow blocking drag is highly sensitive to the critical Froude number, with the peak zonal flow blocking drag for $F_c = 4$ being approximately an order of magnitude greater than that for $F_c = 1$. Comparison of simulations where a different F_c is used for the transition to flow blocking than for the diagnosis of blocked layer depth (shown in Figs. 4(middle right) and (bottom left)) reveal that the drag is reduced more when F_c is altered for the blocking depth calculation then when it is altered for the transition to flow blocking. This indicates that the sensitivity of the drag to F_c via the blocking depth diagnosis is larger than the sensitivity due to the threshold for the onset of blocking. Interestingly if the dependence of blocking depth on Froude number is removed entirely (by setting $Z_b = H$, Fig. 4 bottom right) the zonal drag is only slightly increased compared to the equivalent experiment with F_c for blocking depth set to 4 (Fig. 4 (middle right)). This implies that the effect of setting F_c to such a large value for blocking depth is to make the blocking depth close to the mountain height in all situations where significant blocking drag is parametrized. However, even when the blocking depth is independent of Froude number if the flow blocking transition F_c is set to unity (Fig. 4(bottom right)), the parametrized zonal flow blocking drag is significantly smaller than

that seen in the 5a CONTROL experiment (Fig. 4(top right)).

Attempts to achieve good performance with a smaller F_c by adjusting other tunable parameters (for example by increasing Cd, increasing n_σ and increasing $Z0_{eff}$) met with little success. As a result it is unlikely that it will be possible to find a configuration for the new scheme with $F_c = 1$ which is competitive with the current operational configuration (although it may be possible to find a competitive configuration with $F_c = 2$ if the blocking depth is set to the SSO height and the drag coefficient is increased). There are several possible reasons why a larger value of F_c than would appear physically appropriate may be required in order to get good results:

- The scheme may be compensating for a lack of low-level drag, resulting from another physical process, in the model.
- The scheme may be compensating for a systematic overestimation of the low-level Froude number by the parametrization scheme (either via a systematic overestimation of U_{av}; a systematic underestimation of N_{av}; or an underestimation of H relative to the actual SSO height).
- Having a large value of F_c may be a (crude) way of accounting for variability in low-level Froude number within a grid-box (i.e. if $F_{av} \leq 4$ in a grid-box then somewhere in that grid-box $F \leq 1$ and therefore parametrizing some flow blocking drag is appropriate)

It would be interesting to investigate the reasons for needing to use a larger value of F_c by comparing the output from the parametrization to a high resolution numerical model.

4.3 Tuning parameter 2: Sensitivity to Saturation Froude Number, F_{sat}

In order to investigate the sensitivity to the saturation Froude number, F_{sat}, simulations were run with three values of F_{sat} [0.5, 1.0 (5a CONTROL), 2.0]. Figure 5 shows the zonally averaged zonal gravity wave acceleration with $F_{sat} = 1$ (5a CONTROL) and $F_{sat} = 0.5$. Using the smaller value of F_{sat} leads to larger accelerations throughout the stratosphere, as a smaller proportion of the wave stress is deposited in the troposphere. This means that the peak (point) acceleration at a height of 40 km is increased by $\approx 70\%$. Figure 6 shows the converse scenario where F_{sat} has been doubled. In this case weaker accelerations are seen in most of the stratosphere, however there is an increase in the acceleration seen above the Himalaya at a height of 35 km, which seems to result from less stress being deposited lower down in the stratosphere (around 20 km) although it is unclear why this occurs. By doubling F_{sat} the peak (point) acceleration at a height of 40 km is reduced by $\approx 40\%$. The sensitivity to F_{sat} implies that it is a useful tuning parameter for changing the vertical distribution of gravity wave drag.

4.4 Tuning parameter 3: Sensitivity to n_σ

In order to investigate the sensitivity to n_σ (which controls the SSO mountain height via $H = n_\sigma \sigma$) simulations were run with three values of n_σ [1.5, 2.5 (5a CONTROL), 3.5]. As one would expect

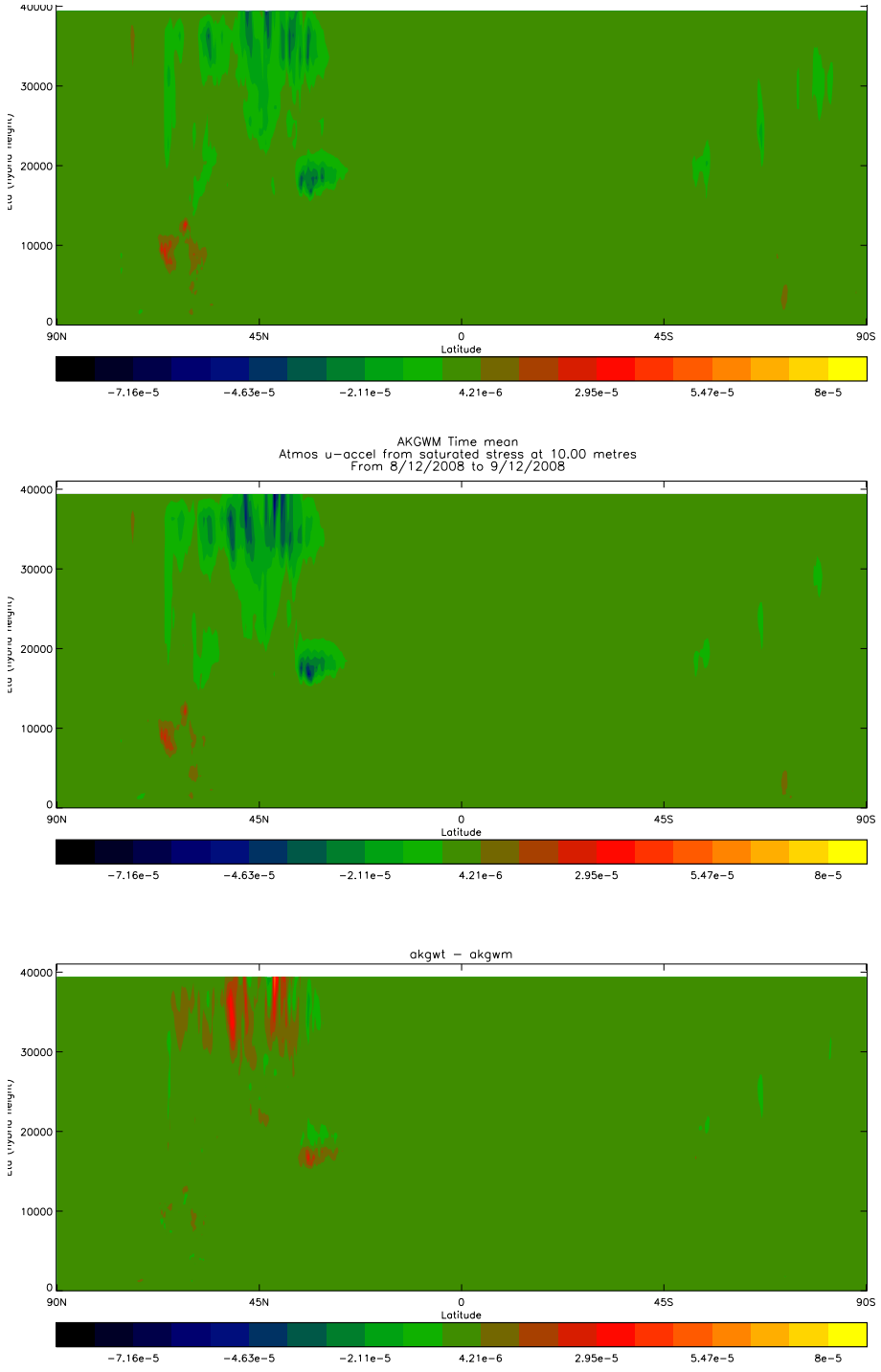

Figure 5: Zonally averaged daily averaged zonal gravity wave accelerations for (top) 5a CONTROL ($F_{sat} = 1$) (middle) $F_{sat} = 0.5$ and (bottom) CONTROL-$F_{sat} = 0.5$.

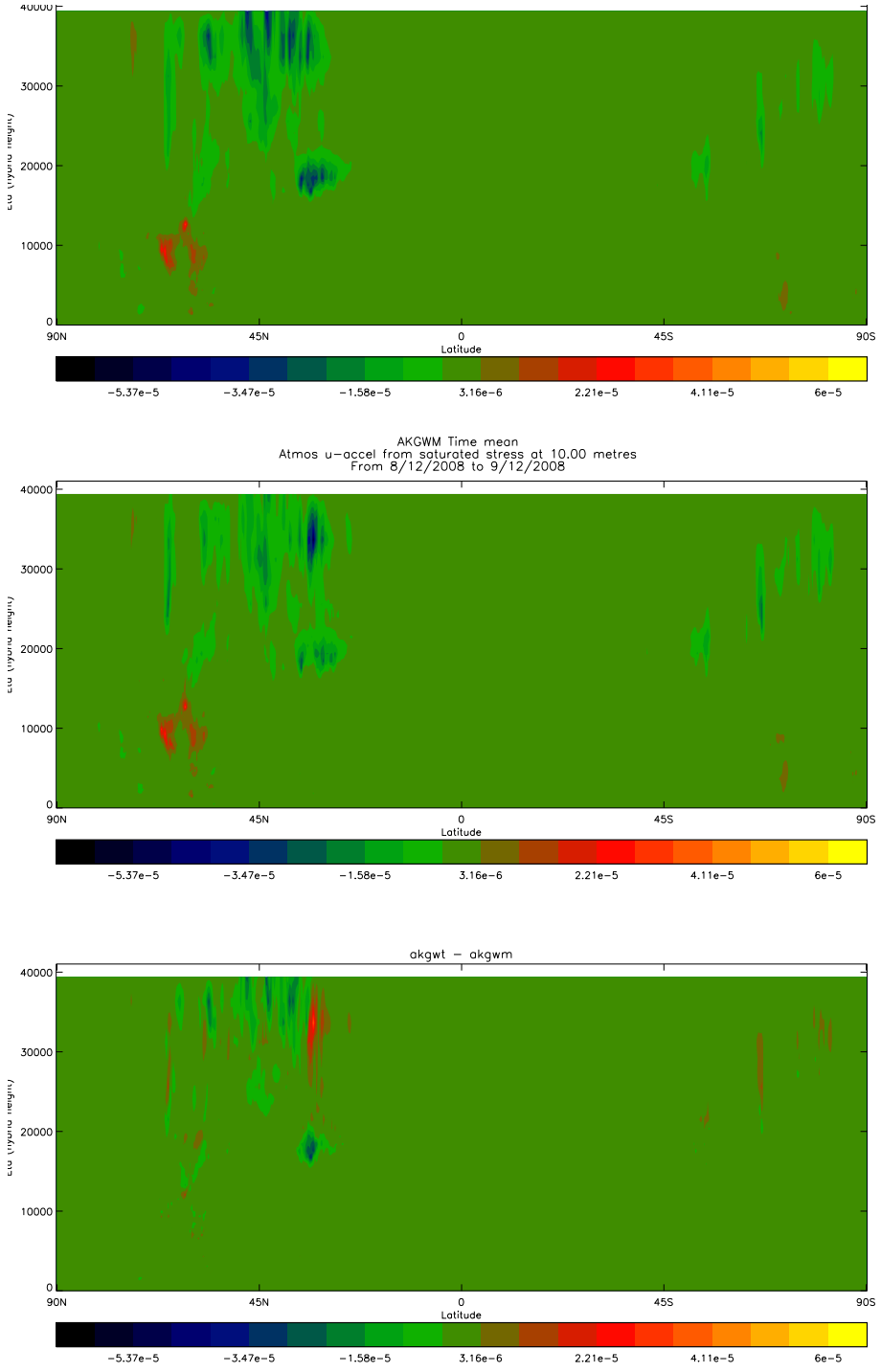

Figure 6: Zonally averaged daily averaged zonal gravity wave accelerations for (top) 5a CONTROL ($F_{sat} = 1$) (middle) $F_{sat} = 2$ and (bottom) CONTROL-$F_{sat} = 2$.

when n_σ is decreased there is a general reduction in the surface stress, however it was found that the flow blocking stress was more sensitive to changes in n_σ than the gravity wave stress. For example the zonal flow blocking accelerations increased (decreased) by $\approx 50\%$ as n_σ was increased (decreased) from 2.5 to 3.5 (1.5). This is illustrated by Fig. 7 which shows the zonally averaged zonal flow blocking accelerations for the 5a CONTROL ($n_\sigma = 2.5$) and a simulation with $n_\sigma = 1.5$. In addition to the significant reduction in the flow blocking accelerations, one observes that the accelerations are restricted to lower heights in the $n_\sigma = 1.5$ simulation. This is a result of significantly shallower blocked layer depths in this simulation (for example a reduction in the maximum Z_b from 2977 m in the 5a CONTROL to 1769 m in the $n_\sigma = 1.5$ simulation). It is worth noting that in some regions (e.g. near the surface at $\approx 80^\circ$ S) the flow blocking accelerations are slightly increased when n_σ is decreased, possibly as a result of changes in the low-level winds and stability (which are averaged over a smaller depth in this simulation) or changes in the low-level flow patterns off-setting the reduction in acceleration due to the smaller SSO mountain heights.

Figure 8 shows the zonally averaged zonal gravity wave accelerations for the 5a CONTROL ($n_\sigma = 2.5$) and a simulation with $n_\sigma = 1.5$. In general gravity wave accelerations are approximately 20% smaller when $n_\sigma = 1.5$ than in the 5a CONTROL. However, modest increases in accelerations are observed in the upper stratosphere at a latitudes of 60°N. This is associated with larger gravity wave surface stresses in Alaska which are in turn associated with stronger depth averaged wind speeds being input to the parametrization. These stronger near surface winds are in turn related to smaller flow blocking stresses in this region (which are only partly offset by an increase in boundary layer wind stress).

To summarise one can broadly increase (decrease) the response of the orographic drag scheme by increasing (decreasing) n_σ, although in some regions the opposite response is observed as a result of feedbacks from different parts of the scheme. Additionally the flow blocking accelerations are much more sensitive to changes in n_σ than the gravity wave accelerations.

In order to determine the (physically) appropriate value of n_σ for a given model resolution one could repeat the analysis of [Wallace et al., 1983] who showed that for an N48 model a value of $n_\sigma = 2$ was sufficient to enclose the significant peaks over major mountain ranges when added to the mean orography height. As stated by [Wallace et al., 1983] one would hope that n_σ would not be too resolution dependent (since as the resolution of the model increases, the mean heights increase while the standard deviation decreases), however it is entirely possible that a slightly smaller (or larger) value could be most appropriate at modern NWP resolutions.

4.5 Option 1: Sensitivity to discarding three SSO parameters

The squared grid-box average gradient parameters, σ_{ij}, are used directly by the 4a scheme and indirectly by the 5a scheme, where they are used to derive the slope, anisotropy and orientation of the SSO. Research by A. Brown and S. Webster (personal communication) indicates that σ_{ij}

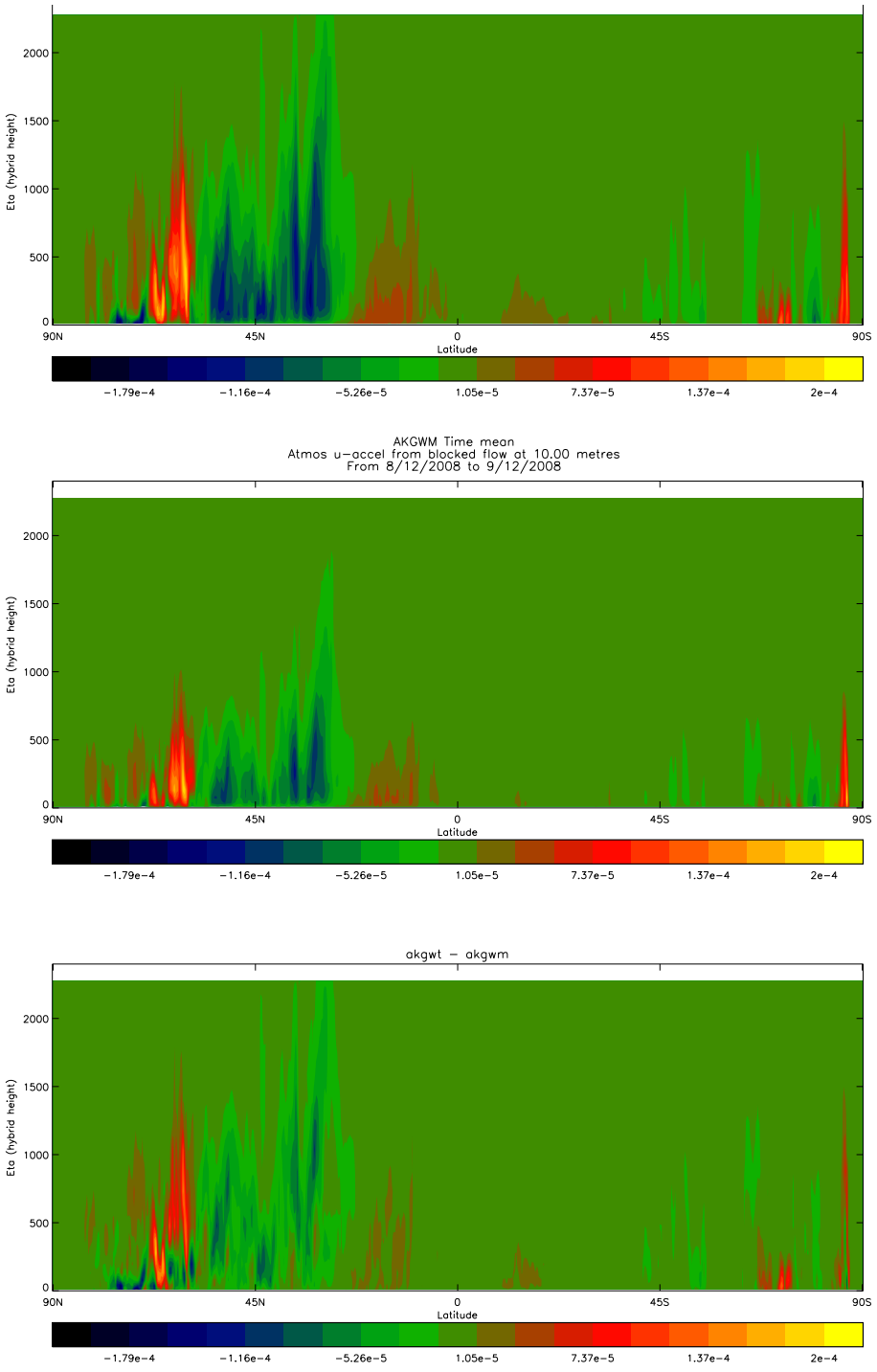

Figure 7: Zonally averaged daily averaged zonal flow blocking accelerations for (top) 5a CONTROL ($n_\sigma = 2.5$) (middle) $n_\sigma = 1.5$ and (bottom) CONTROL-$n_\sigma = 1.5$.

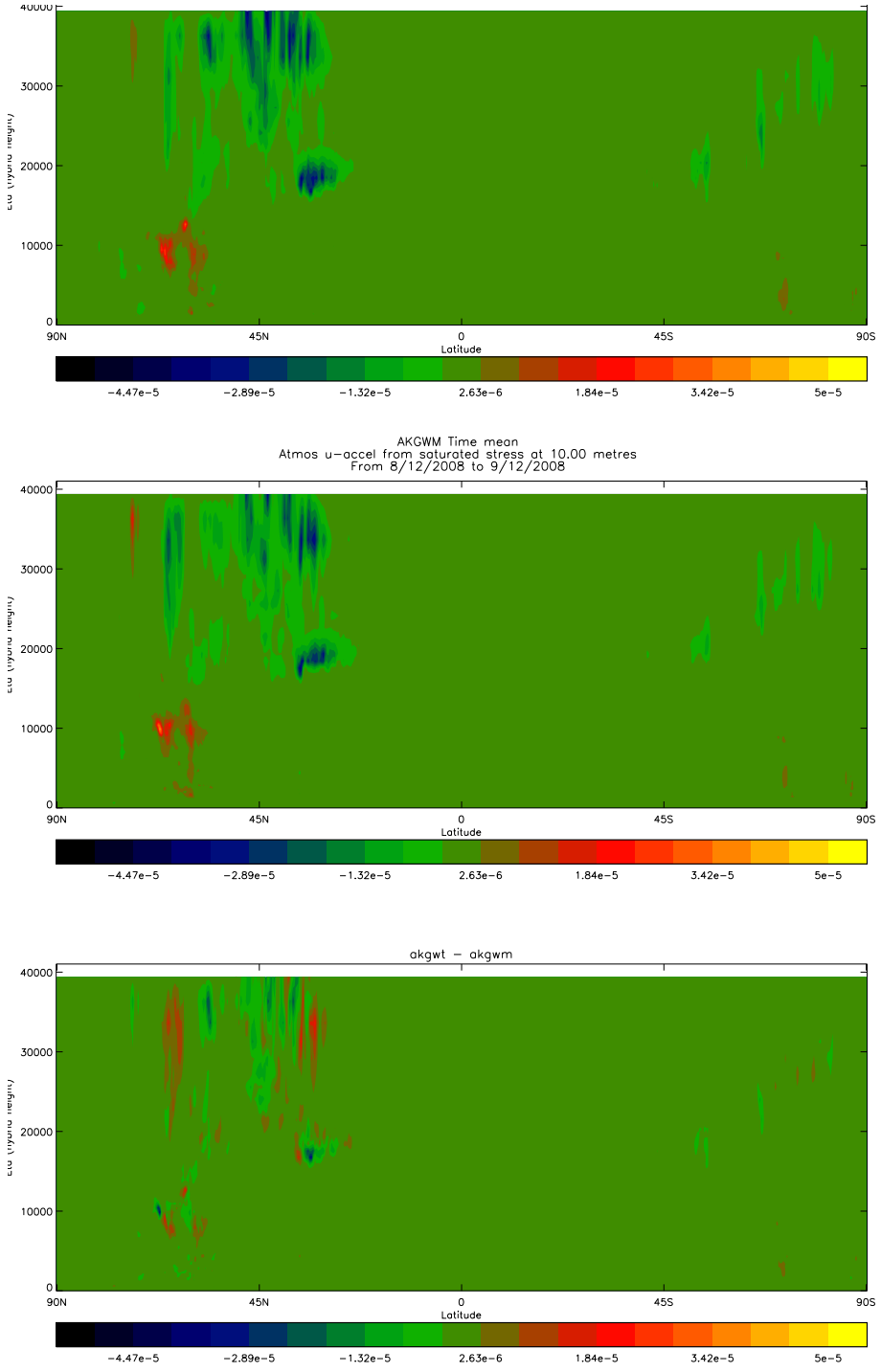

Figure 8: Zonally averaged daily averaged zonal gravity wave accelerations for (top) 5a CONTROL ($n_\sigma = 2.5$) (middle) $n_\sigma = 1.5$ and (bottom) CONTROL-$n_\sigma = 1.5$.

do not converge and become noisy as the resolution of the input data is increased, which could introduce undesirable numerical noise into the forecast model. Additionally it has not been clearly demonstrated that these parameters contain useful information about the underlying topography at current NWP resolutions. Therefore some work has been done to assess whether it might be possible to discard this information. Tests have been done to look at the effect of eliminating σ_{ij} by setting the SSO parameters as follows: anisotropy, $\gamma = 1$; orientation, $\Psi = 0$; and slope, $\alpha = H/(0.25\Delta x$ (where Δx is the grid spacing in the zonal direction). The settings for anisotropy and orientation are equivalent to assuming that all of the SSO is made up of isotropic mountains. Using these settings the only SSO parameter required by the scheme is the standard deviation of the orography, σ, which converges as the resolution is increased and is not noisy at high resolution.

Figure 9 shows the slope calculated using the standard calculation (Fig. 9(top)) and using the alternative calculation (Fig. 9(bottom)). The value of 0.25 used in the denominator was chosen in order to achieve similar values of α over the major mountain ranges to that given by the standard calculation. However, the eye is drawn to significant differences in α in the polar regions (which arise from the decreased zonal grid spacings in these regions), these differences mean that the maximum slope from the alternative calculation is five times larger than the maximum slope in the original calculation.

Figure 10 shows the surface stress in the 5a CONTROL and in a simulation using the alternative SSO parameters (but otherwise having an identical set-up to the 5a CONTROL). The global distribution of stress looks similar in the two simulations (although the surface stresses are generally slightly larger using the alternative formulation).

Figure 11 shows the zonally averaged zonal flow blocking accelerations for the 5a CONTROL and the alternative SSO parameter simulation. Clearly the zonally averaged flow blocking accelerations are very similar, although the difference plot reveals that the accelerations in the polar regions are somewhat stronger (consistent with the significantly larger slopes seen in these regions in Fig. 9). Consistent with this result one only observes significant differences in the low-level Froude number over Antarctica (not shown). Differences in zonally averaged gravity wave accelerations between these two simulations, shown in Fig. 12, are more significant. The peak zonally averaged gravity wave acceleration is increased by a factor of 1.8 and, although the spatial distribution of accelerations is unchanged over most of the globe, accelerations are disproportionately higher at high latitudes in the southern hemisphere using the alternative SSO parameters. Note that comparison of the gravity wave accelerations at 40 km (not shown) reveals an increase in accelerations over the Himalayan region but does not indicate the presence of any significant accelerations at high latitudes.

The results from the alternative SSO simulation are fairly encouraging, therefore this option was tested more fully by running a case study suite. This will be discussed further in section 5.3.

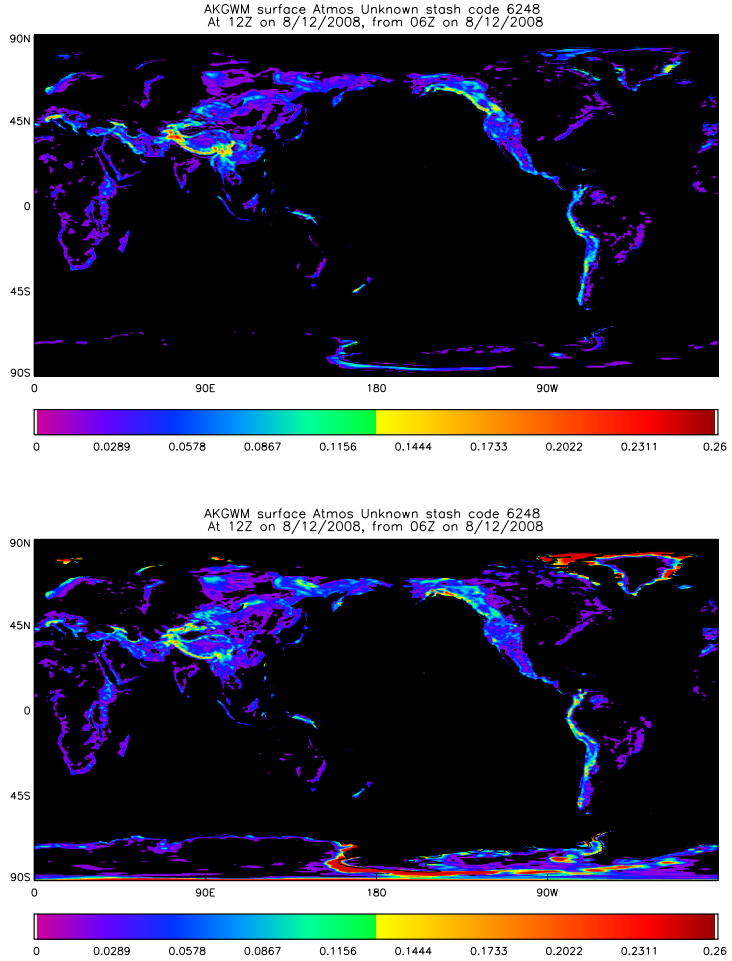

Figure 9: The slope, α, input into the parametrization scheme (top) 5a CONTROL (i.e. using LM97 SSO calculation) and (bottom) using $\alpha = H/(0.25\Delta x)$.

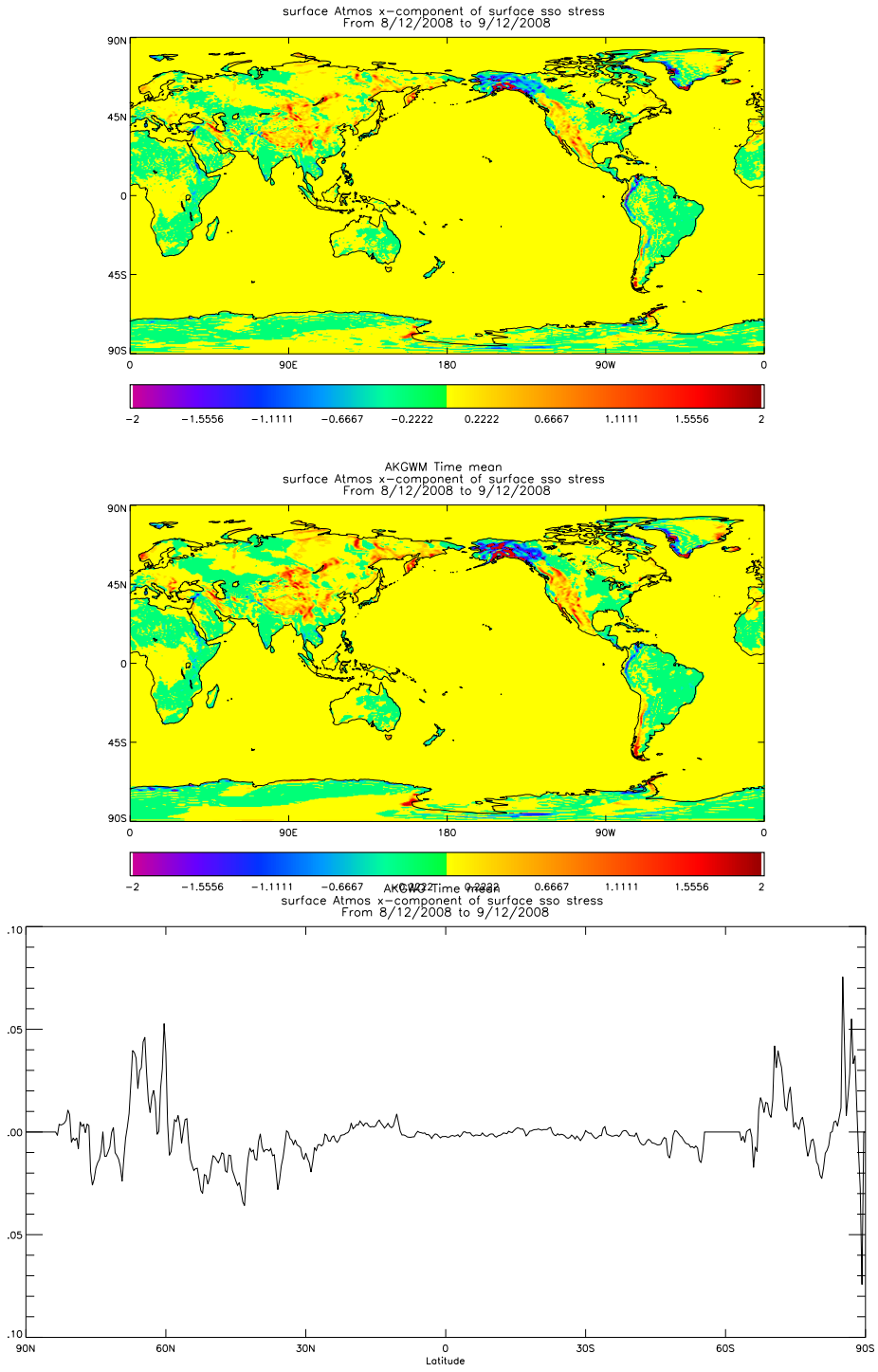

Figure 10: Daily averaged zonal surface stress (gravity wave + flow blocking) for (top) 5a CONTROL (middle) Alternative SSO parameters ($\gamma = 1$, $\Psi = 0$, $\alpha = H/(0.25\Delta x)$ and (bottom) Zonally averaged difference between 5a CONTROL and alternative SSO parameters.

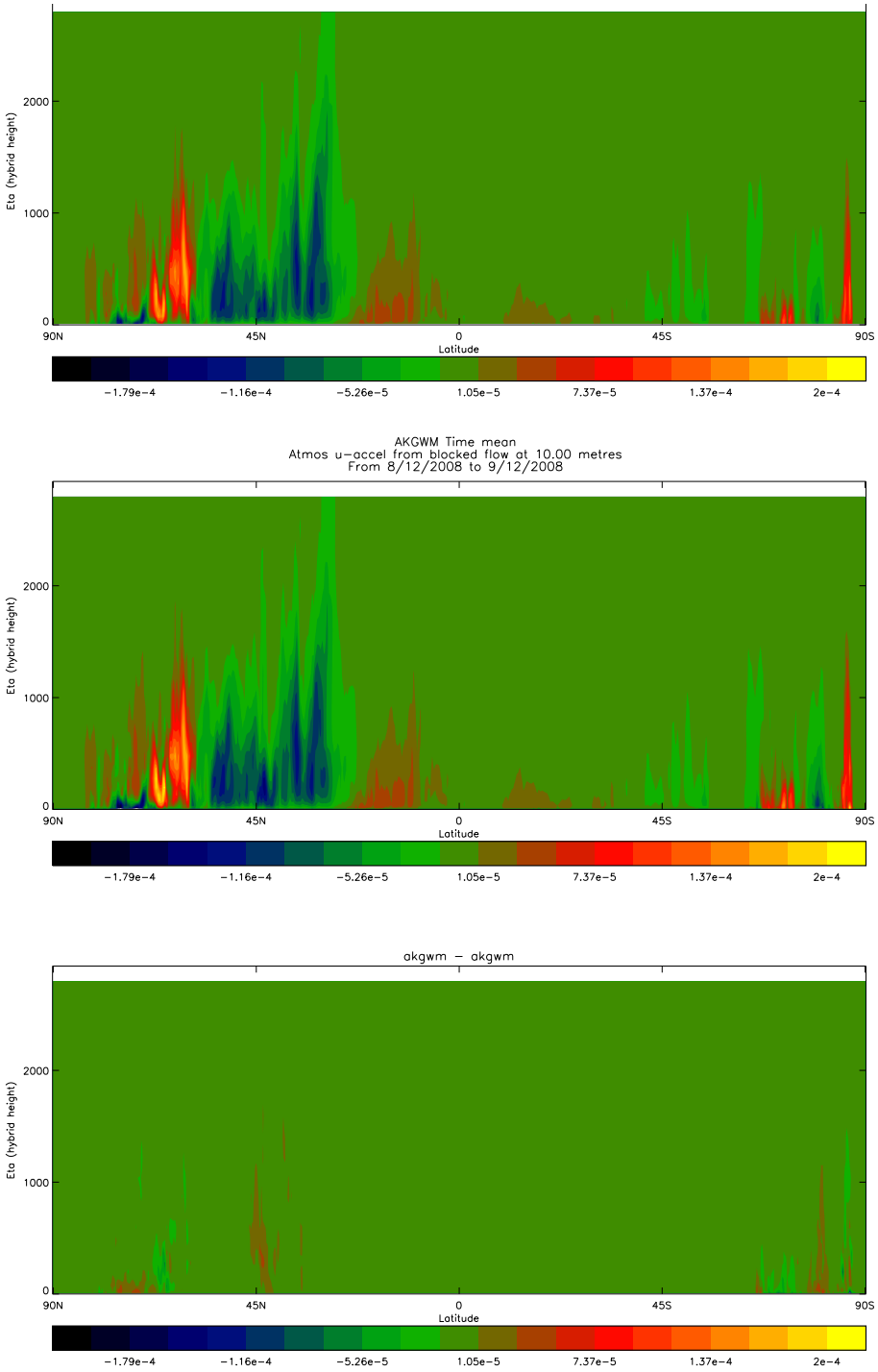

Figure 11: Zonally averaged daily averaged zonal flow blocking accelerations for (top) 5a CONTROL (middle) Alternative SSO parameters ($\gamma = 1$, $\Psi = 0$, $\alpha = H/(0.25\Delta x)$ and (bottom) CONTROL-Alternative SSO

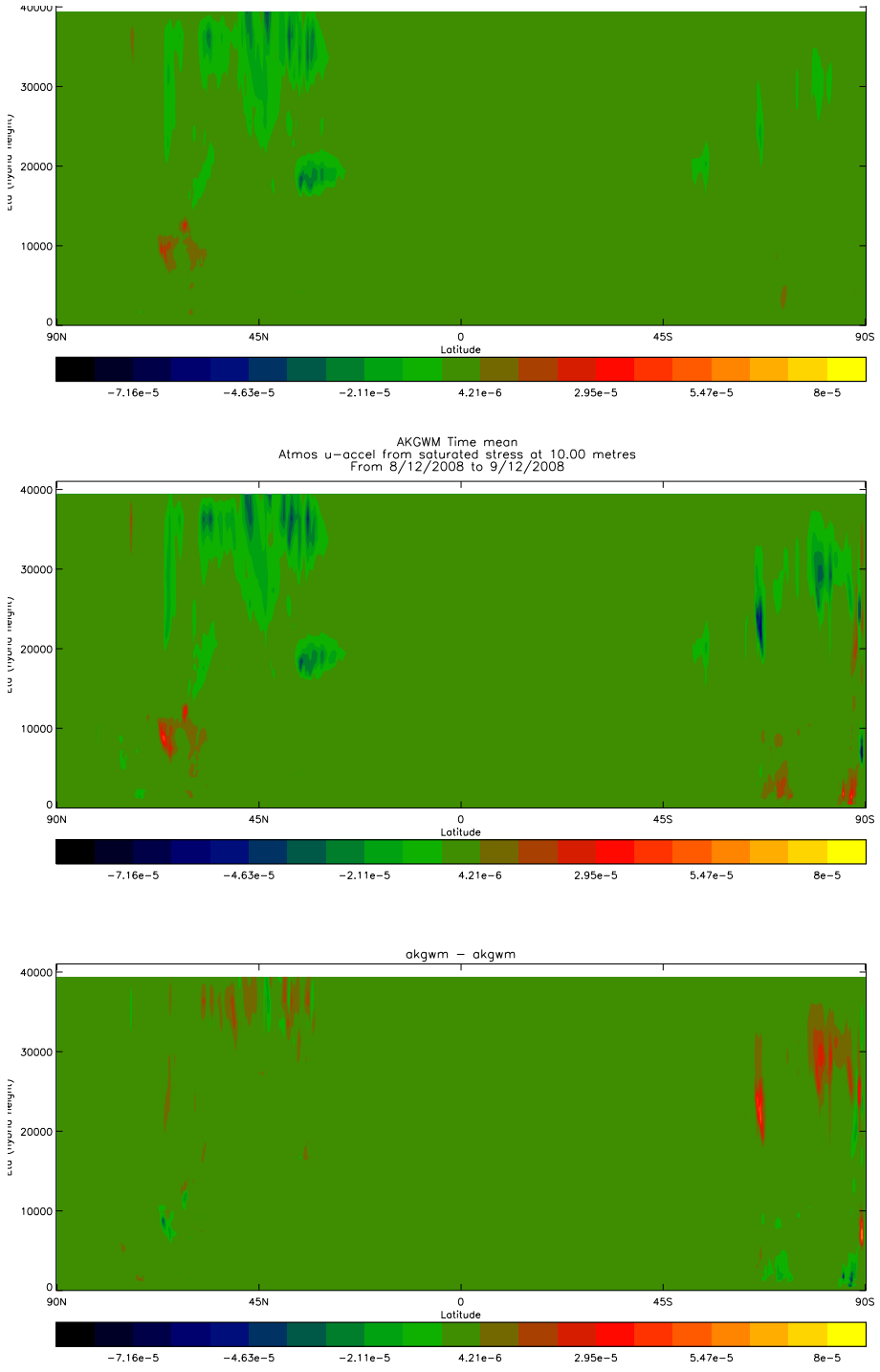

Figure 12: Zonally averaged daily averaged zonal gravity wave accelerations for (top) 5a CONTROL (middle) Alternative SSO parameters ($\gamma = 1$, $\Psi = 0$, $\alpha = H/(0.25\Delta x)$ and (bottom) CONTROL-Alternative SSO

4.6 Option 2: Sensitivity to smoothing drag over a vertical wavelength

The main effect of smoothing the gravity wave drag over a vertical wavelength is to allow a modest increase in launch amplitude of waves (here from $G = 0.8$ to $G = 1$) without increasing the stratospheric drag. For the tests described here the standard settings for the parameters which control the smoothing were set to $\lambda z_{min} = 100$ m, $\lambda z_{max} = 10000$ m and $\chi = 1.0$. Figures 13 (top) and (middle) show the zonally averaged daily averaged gravity wave accelerations for two versions of the 5a scheme, one without smoothing and with $G = 0.8$ and one with smoothing and with $G = 1$. These accelerations are clearly similar, a fact which is confirmed by Figure 13 (bottom) which shows the difference between the two versions (no smoothing - smoothing), using a colour scale has one tenth of range of that used for Figures 13 (top) and (middle), which show only small changes in the upper stratospheric accelerations (near 40 km) despite the increase in the launch amplitude.

Figure 14 shows the daily averaged gravity wave accelerations at a height of 40 km (the highest height at which gravity wave accelerations are parametrized). Comparison of the results in 5a CONTROL with those in 5a SMOOTH reveal that in 5a SMOOTH the accelerations at $z = 40$ km are increased by a small amount over many broad regions (e.g. Rockies, Scandinavia) with more significant increases in accelerations over a few small areas (e.g. North-Eastern Canada and Kamchatka Peninsula) presumably as a result of the increase in G. However the most significant effect of the smoothing is to decrease the accelerations over the Himalayas (which leads to a decrease in zonal mean acceleration at 45° N at 40 km, see Fig. 13).

As part of the investigation into the sensitivity to smoothing, tests were done to look into the sensitivity to the various tunable parameters that control the smoothing, namely λz_{min}, λz_{max} and χ. In each case the effect on zonal mean gravity wave accelerations, zonal mean flow blocking accelerations and gravity wave accelerations at 40 km was investigated (note: flow blocking accelerations were investigated since λz_{min} and λz_{max} are used to limit the range of values that U/N takes in the calculation of the depth-averaged low-level Froude number, F_{av}). It was found that the results were insensitive to halving or doubling λz_{max}, however significantly increasing λz_{min} (from 100 m to 500 m) led to an increase in the zonal mean gravity wave acceleration of about 10% and increased the peak gravity wave acceleration at 40 km by 43%. Increasing λz_{min} also led to an increase in the zonal mean flow blocking acceleration between 50° N to 70° N of up to 10% at low-levels (i.e. below a height of 500 m). However $\lambda z_{min} = 500$ m is probably outside the physical bounds of values which one would want to set this parameter, and smaller changes in λz_{min} had little effect.

For gravity waves the strongest sensitivity was seen to the fraction of the wavelength that the accelerations are smoothed over, χ (note this parameter does not influence flow blocking accelerations). Halving (doubling) χ led to a significant decrease (increase) in zonal mean accelerations and a significant increase (decrease) in peak accelerations at 40 km of $+40\%$ (-25%). This effect is illustrated in Fig. 14 which shows the zonal mean accelerations for Fig. 14(top) 5a SMOOTH ($\chi = 1$) and Fig. 14(middle) as 5a SMOOTH but $\chi = 2$, with the difference shown in Fig. 14(bottom). It is

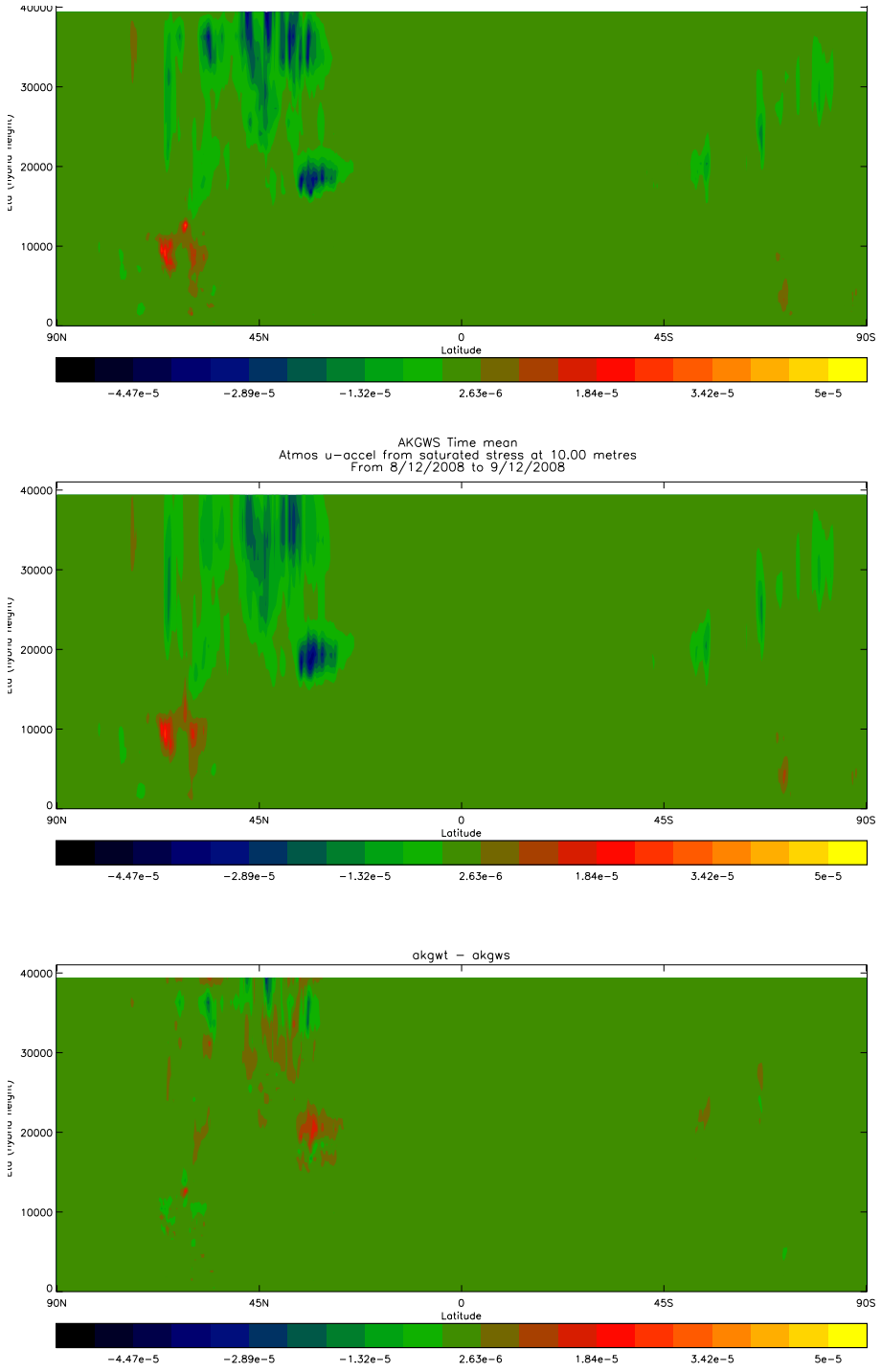

Figure 13: Zonally averaged daily averaged zonal gravity wave accelerations for (top) 5a CONTROL (middle) 5a SMOOTH and (bottom) CONTROL-SMOOTH (note that the colour scale has one tenth of range of that used for the two upper plots).

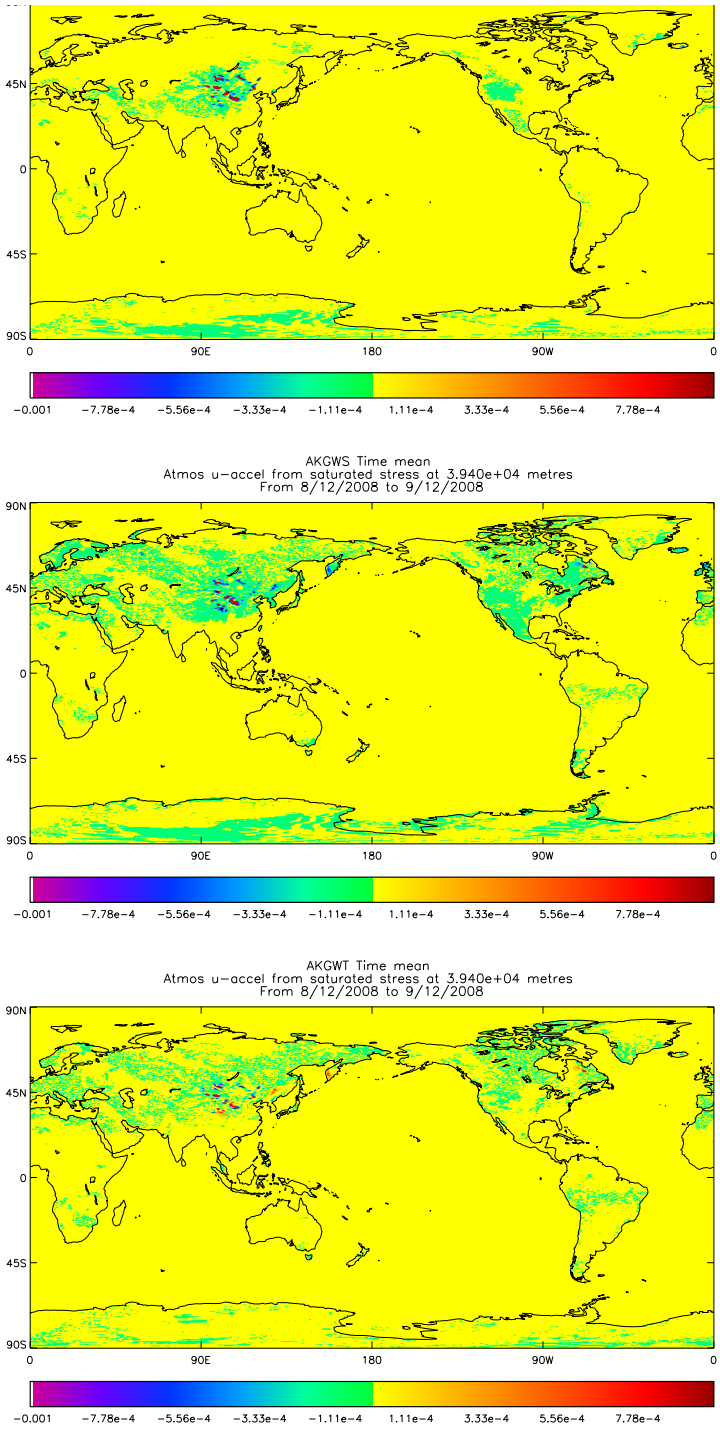

Figure 14: Daily averaged zonal gravity wave accelerations at 40km for (top) 5a CONTROL (middle) 5a SMOOTH (bottom) CONTROL-SMOOTH.

clear that setting $\chi = 2$ significantly reduces the peak zonal mean accelerations. Therefore χ is a useful parameter for tuning the vertical distribution of gravity wave drag (when smoothing is on).

4.7 Option 3: Sensitivity to non-hydrostatic correction

In order for the non-hydrostatic correction to have a significant effect on the zonal mean gravity wave accelerations, one must set the ratio of vertical to horizontal group velocities, β, to a value of order unity (or less). Here we show the effect of the non-hydrostatic correction when $\beta = 1$. However it is worth mentioning beforehand that this value seems unphysically large as it implies an average propagation angle for the wave packets of 45° and is much larger than the average β calculated from the dynamical calculation ($\beta \sim O(100)$). For typical values (slope $\alpha = 0.01$, $H = 1000$m, $U = 10$ms^{-1} and $N = 0.01$s^{-1}) the average β from the dynamical calculation implies that a typical gravity wave horizontal wavelength is ≈ 630 km which seems far too large, given that the mid latitude grid spacing is 40 km. This unphysically large typical wavelength suggests that the formulation of the dynamical β needs further thought as one would hope for a typical wavelength in the range of $20 - 40$ km. In contrast, $\beta = 1$ implies a typical horizontal wavelength of 6.3 km which is at the lower limit of wavelengths that are forced by the sub-grid scale orography (as the orography has been filtered to remove length scales shorter than 6 km). Possibly the non-hydrostatic formulation (as it stands) could be used if the scheme was run a second time each time-step with the non-hydrostatic option switched on and a different set of orography ancillaries which only contained information on scales between, say, $1 - 10$ km.

The combination of the non-hydrostatic correction with $\beta = 1$ and the smoothing means that the gravity wave launch amplitude can be increased significantly (from $G = 1$ for smoothing without non-hydrostatic correction to $G = 2$ for smoothing with the non-hydrostatic correction) without significantly increasing the drag at 40 km. Figure 16 shows the zonally averaged gravity wave accelerations for the 5a CONTROL and for a run with both smoothing and the non-hydrostatic correction switched on (SMOOTH_NH). While SMOOTH_NH gives enhanced accelerations over the majority of the atmosphere (due to a combination of increased momentum flux deposition and increased launch amplitudes), above 35 km the accelerations are reduced at some latitudes and enhanced at others leading to only a small overall increase in zonal mean accelerations.

4.8 Summary of results from running the NWP model for a single case

In this section the 5a scheme has been perturbed in various ways in order to understand the sensitivity to three tuning parameters and three more significant changes. For the basic configuration of the scheme it has been shown that F_{sat} is an effective tuning parameter for the vertical distribution of gravity wave acceleration. The tuning constant, n_σ, which determines the SSO mountain height (via $H = n_\sigma \sigma$) has been shown to have a stronger effect on the flow blocking accelerations than the gravity wave accelerations. A strong sensitivity on the critical Froude number, F_{crit}, was observed

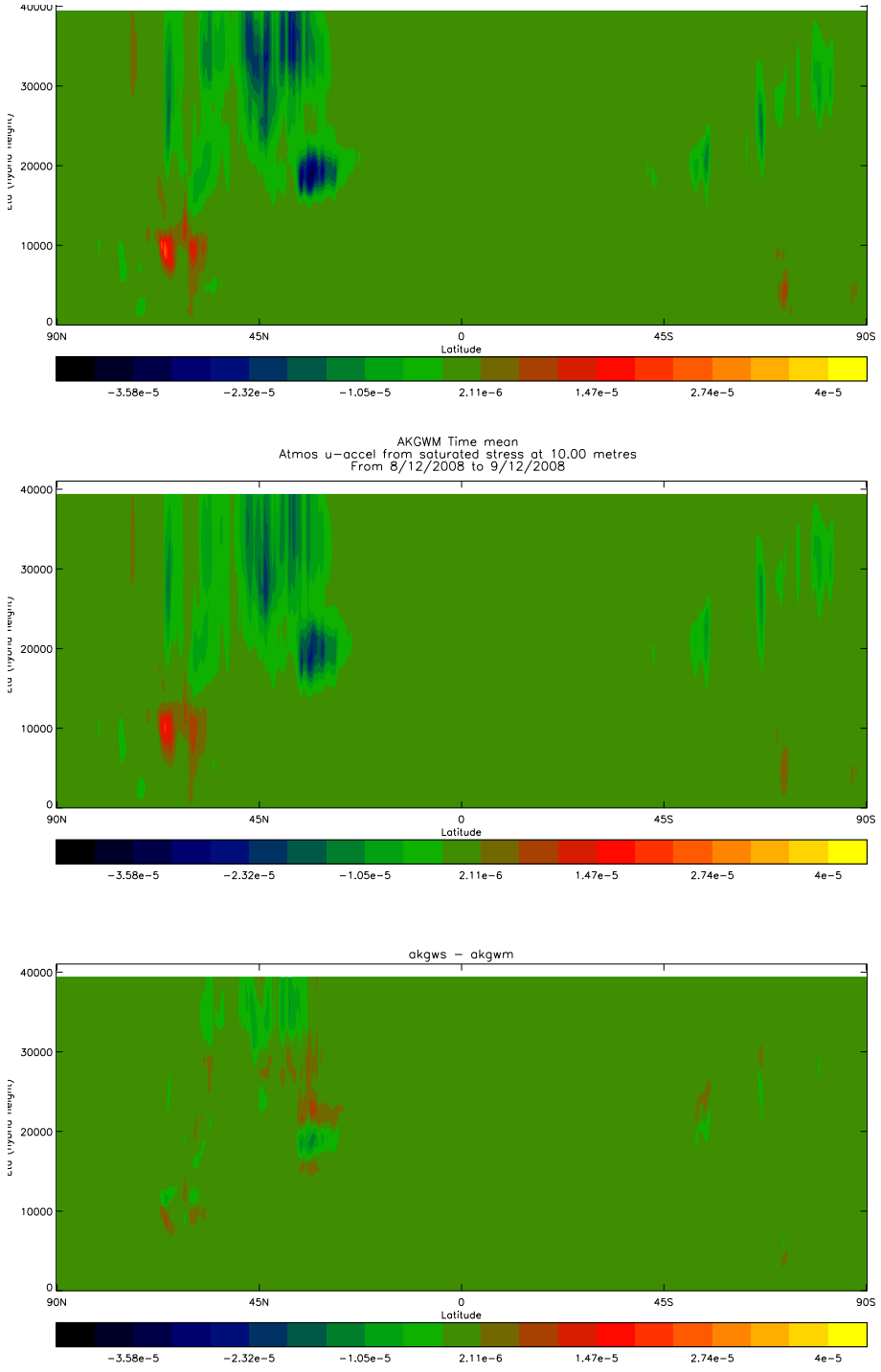

Figure 15: Daily averaged zonal gravity wave accelerations at 40km for (top) 5a SMOOTH ($\chi = 1$) (middle) as 5a SMOOTH but $\chi = 2$ (bottom) Difference 5a SMOOTH($\chi = 1$)-SMOOTH($\chi = 2$).

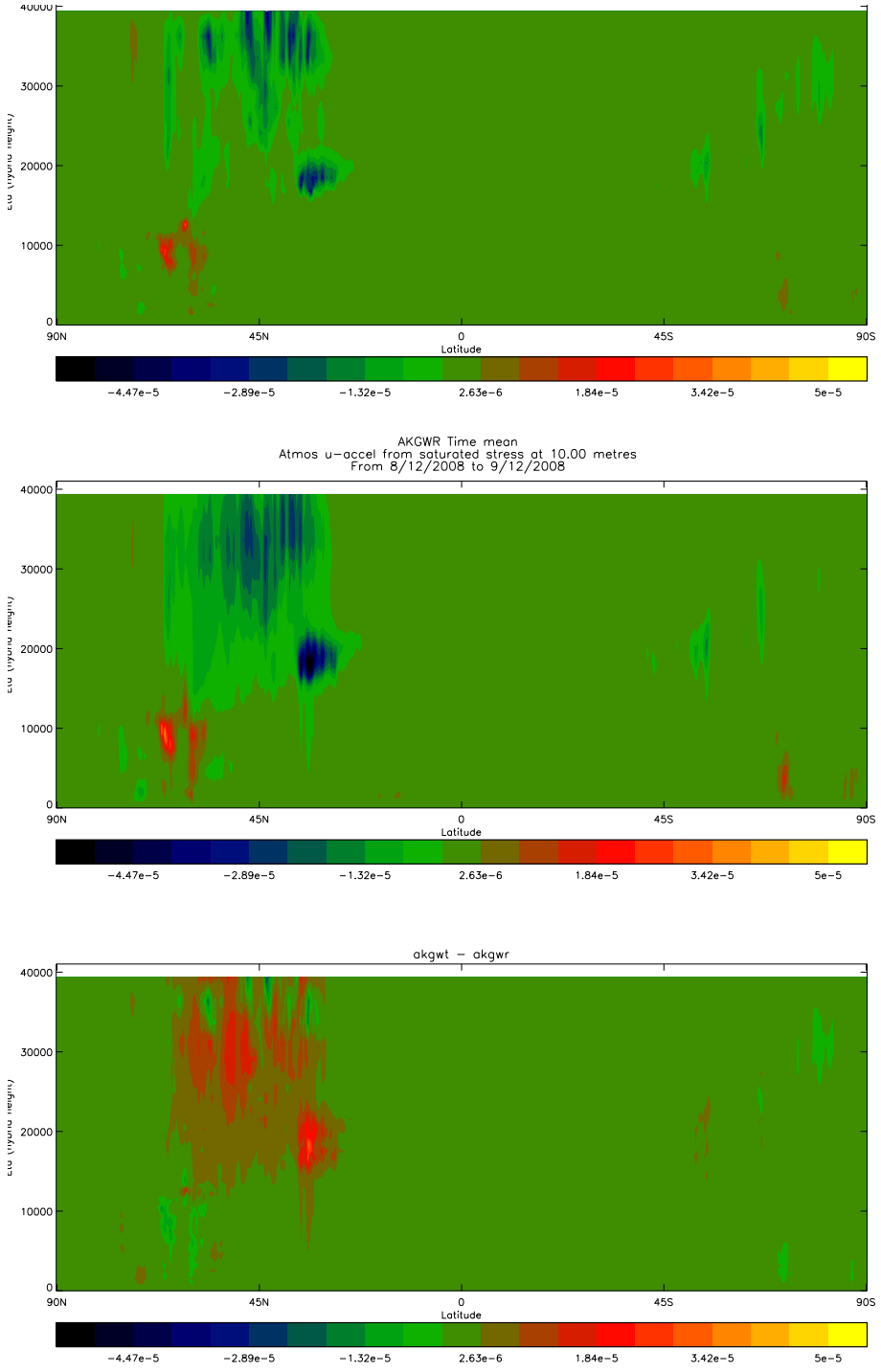

Figure 16: Zonally averaged daily averaged zonal gravity wave accelerations for (top) 5a CONTROL (middle) 5a SMOOTH_NH and (bottom) Difference CONTROL-SMOOTH_NH.

with decreases in F_{crit} (from the default setting of 4 to 1) seen to significantly decrease the flow blocking drag. As yet it has not been possible to find a competitive configuration of the 5a scheme with $F_{crit} = 1$ which is disappointing given that one of the reasons for moving to a new scheme was to try to set F_{crit} to a more physically appropriate value. However, it is plausible that we require a larger value of F_{crit} than would be expected from theoretical considerations in order to account for the variability in low-level Froude number in a grid box (arising from effects such as variable low-level flow and stability or de-coupled flow in valleys). This hypothesis is worthy of further investigation.

The sensitivity to three more significant changes was also assessed. First, it has been shown that discarding the SSO parameters based on the grid-box mean gradients (σ_{ij}) and replacing them with either fixed values (anisotropy and orientation) or values dependent on the standard deviation of the SSO (slope) has some potential, although some significant differences are observed in the high latitudes. Therefore this set-up will be assessed in more detail in NWP case study tests. If this set-up can achieve competitive skill scores when compared to the operational scheme then it would be beneficial to use it due to the lack of convergence of the grid-box mean gradients (σ_{ij}) with increasing horizontal resolution. Second, it has been shown that smoothing the drag over a vertical wavelength seems to be a viable option since it does not appear to degrade any model fields and it allows the amplitude of the gravity waves launched (set by G) to be increased without significantly increasing the drag at 40 km. The amount of smoothing can be tuned via χ which determines the fraction of a vertical wavelength over which the drag is to be deposited. Increasing χ would allow G to be increased further without increasing the drag at 40 km. It is possible that using the smoothing option could allow the gravity wave drag to be switched on above 40 km (at present it is switched off in order to prevent large accelerations being applied at single grid points in the upper stratosphere which affects model stability). Therefore in the case study tests, the impact of smoothing will be assessed and the possibility of switching gravity wave drag on above 40 km will be investigated. Third, it has been seen that to see a significant effect from the non-hydrostatic correction one must set the ratio of vertical to horizontal group velocities to a value close to unity (i.e. a propagation angle of 45°) which seems unphysical. I believe that this option is worth further consideration, but that more thought is required in it's formulation and/or usage before it warrants more detailed testing. Therefore the non-hydrostatic option will not be pursued further in this report.

It is worth noting that as yet the sensitivity to various minor parameters (Nsq_neu,Zav_converge and Zav_iterate) which have been set somewhat arbitrarily has not yet been assessed (although one would hope that only small sensitivities would be seen to these parameters). Also it would be useful to assess the sensitivity to the effective roughness length, $Z0_{eff}$, in order to understand the effect of changing this parameter from the default setting in the 4a scheme.

5 Results from NWP case study tests of the new scheme

In order to assess the performance of the new scheme NWP case study tests were run for the N320L70 model. Results were compared to output from the control set-up (Parallel Suite 25, using the 4a scheme). For each case study twenty five-day forecasts were run with five forecasts from each of the following seasons: summer 2008, winter 2008/2009, summer 2009, winter 2009/2010. These forecasts were then compared to observations (both surface observations and radiosondes) and the analysis.

The case study tests which will be discussed in this report are:

- CONTROL - 4a scheme (Parallel Suite 25, using 40km filtering for sub grid-scale orography, no gravity wave drag above 40 km).
- 5a CONTROL - as CONTROL except 5a scheme, using 6km filtering for sub-grid scale orography, $Cd = 10$, $G = 0.8$, $Z0_{eff} = 0.45$, Smoothing off, no gravity wave drag above 40 km.
- 5a SMOOTH - as 5a CONTROL except $Cd = 12$, $G = 1$, Smoothing on($\chi = 1$) (and using 40km filtering for SSO).
- 5a GWD TO LID - as 5a SMOOTH except gravity wave drag applied above 40km.
- 5a BLOCK - as 5a SMOOTH except $Z_b = H$ for flow blocking drag only with a normal Z_b used for cut-off mountain calculation for gravity wave drag.
- 5a ALT SSO - as 5a SMOOTH except alternative SSO definitions used (no σ_{ij}, anisotropy, $\gamma = 1$; orientation, $\Psi = 0$; and slope, $\alpha = H/(0.25\Delta x$ (where Δx is the grid spacing in the zonal direction).

Sections 5.1 and 5.2 will focus on comparing the CONTROL and the 5a CONTROL with observations and analyses. The other tests will be discussed in section 5.3. Note that these tests were mistakingly run with 40 km filtering for the SSO, however this does not affect the conclusions drawn in this report. Finally section 6 highlights the current recommended set-up, discusses the computational cost of the 5a scheme and details the next stages of testing of the 5a scheme.

5.1 Verification against observations and analyses: 5a CONTROL

Figure 17 shows forecasts compared to analyses for mean sea level pressure in the Southern Hemisphere for the 5 cases from summer 2009 (i.e. during the austral winter) for four set-ups: CONTROL (red); 5a CONTROL (blue); 5a SMOOTH (green); 5a GWD TO LID (yellow). For this section we shall focus on differences between the CONTROL and the 5a CONTROL. Figure 17 suggests that there is a modest improvement in the bias in all of the 5a set-ups compared to the CONTROL (top figures) and the route-mean-square (rms) error is improved by an average of 3% compared to the

CONTROL (bottom figures). Figure 18 is the same as Fig. 17 except the comparison is against surface observations instead of analyses. Comparison of Figs 17 and 18 reveals that the reduction in bias is a consistent signal regardless of whether the comparison is done against analyses or observations. However the improvement in the rms error is less consistent with good agreement between the two methods of comparison only achieved at the medium range (T+72, T+96). Assessment of the schemes for the same region for summer 2008 reveals a consistent signal, i.e. near neutral rms error with an improvement in the bias when comparing the 5a scheme to the CONTROL.

Figure 19 shows forecasts against analyses for wind speed at T+24 for the same period and location. The route-mean-square error is near neutral (bottom figures) while the 5a scheme gives modest improvements in the bias between 850 hPa and 300 hPa and a very small degradation in the bias above 300 hPa (top figures). Figure 20 is the same as Fig. 19 except here the forecasts are compared to sonde observations (rather than the analyses). Figure 20 suggests that the 5a scheme is near neutral in terms of both bias and rms error (i.e. the differences in the bias seen in Fig. 19 are not evident when the results are assessed against sonde observations). Assessment of the schemes for the same region for summer 2008 reveals a near neutral rms error and slight improvement in the bias when comparing the 5a scheme to the CONTROL. In summary, in the southern hemisphere in the austral winter the 5a scheme appears to perform at least as well as the CONTROL and display a consistent improvement in the mean sea level pressure bias and a slightly less consistent improvement in the bias in the wind speed between 850 hPa and 300 hPa.

Figure 21 shows forecasts compared to analyses for mean sea level pressure in the Northern Hemisphere for the 5 cases from winter 2008/2009. Consistent with the results from the southern hemisphere in the austral winter, Fig. 21 indicates a reduction in the bias (top figures). However, the signal from the rms error is more mixed with a degradation in performance at T+24 of $\approx 3\%$ and neutral performance at medium and long range. Comparison of the same field against surface observations (not shown) is inconsistent in several ways. First, the bias against observations is of opposite sign so the 5a scheme degrades the bias (the bias against analysis was improved). Second, the degradation in rms error at T+24 is not seen when comparing against observations although at longer ranges performance is near neutral as seen in the comparison against analyses. Figure 22 is the same as Fig. 21 except the results are plotted for winter 2009/2010. For this season the bias is again reduced when compared to analyses (Fig. 22) but increased when compared to surface observations (not shown). The rms error against analyses (Fig. 22) implies a modest degradation in performance, with the error bars indicating a degradation of between 2% and 7% at T+120. This signal is also seen when comparing to sonde observations (not shown), although the error bars are larger indicating a degradation in rms error of between 0% and 9% at T+120.

Figure 23 shows forecasts at T+24 compared to analyses for wind speed in the northern hemisphere in winter 2008/2009. A significant improvement in the bias from 850hPa to 200hPa is seen, with the bias approximately halved, although there is a small degradation in the rms error of $\approx 2\%$ at 850 hPa. Comparison against sonde observations (not shown) suggests that the improvement

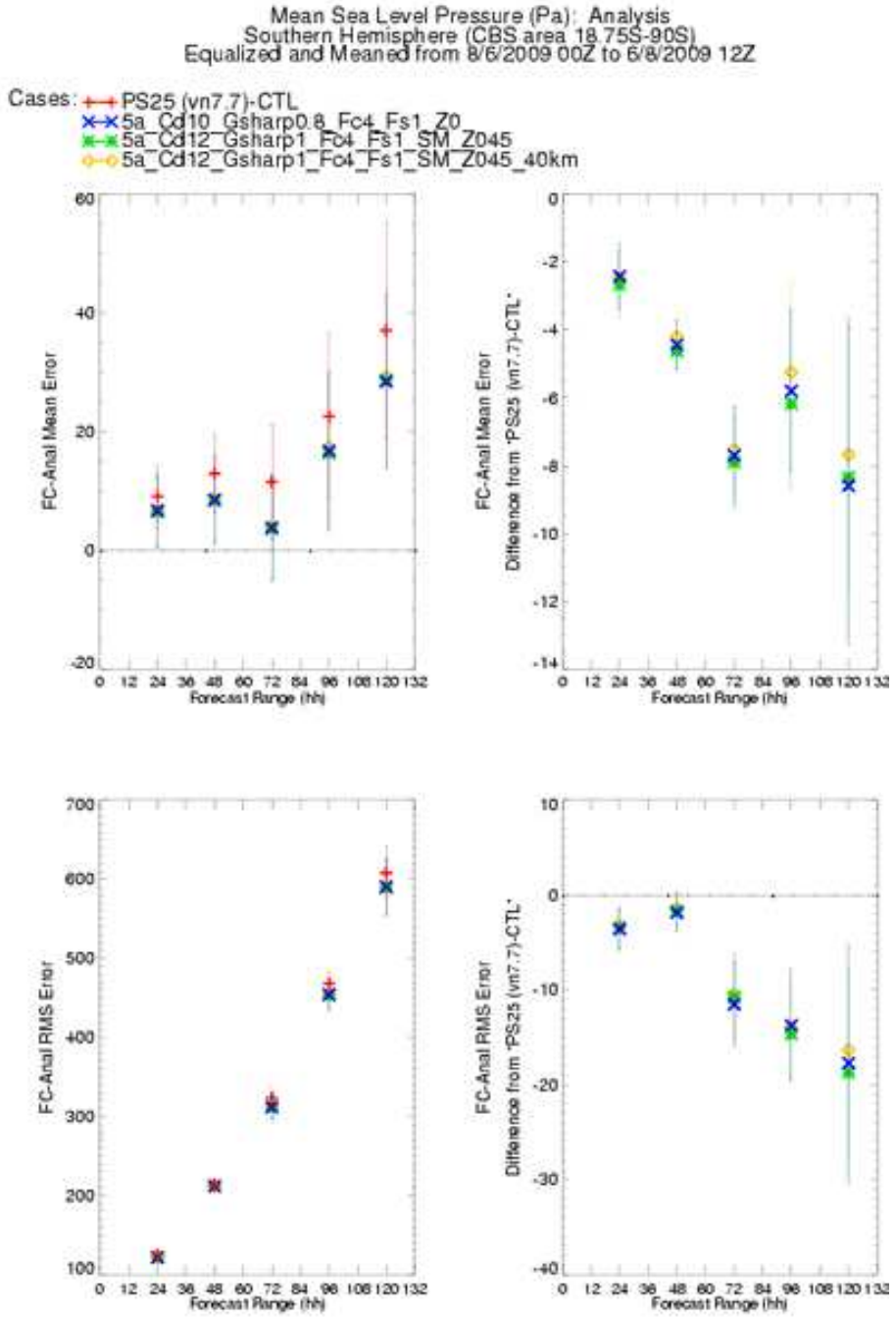

Figure 17: Forecasts compared to analyses for mean sea level pressure in the Southern Hemisphere in Summer 2009.

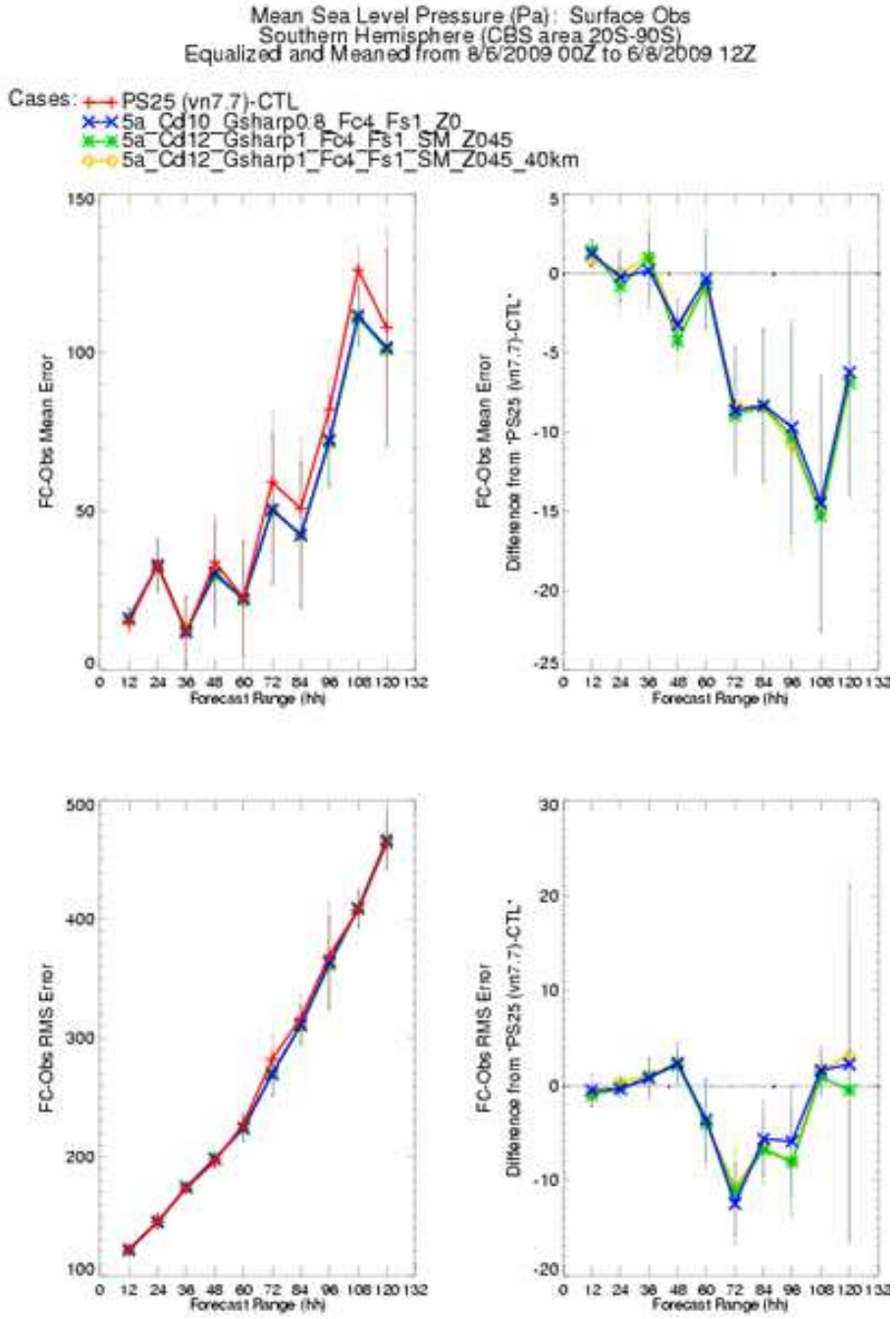

Figure 18: As Fig. 17 but comparison against surface observations.

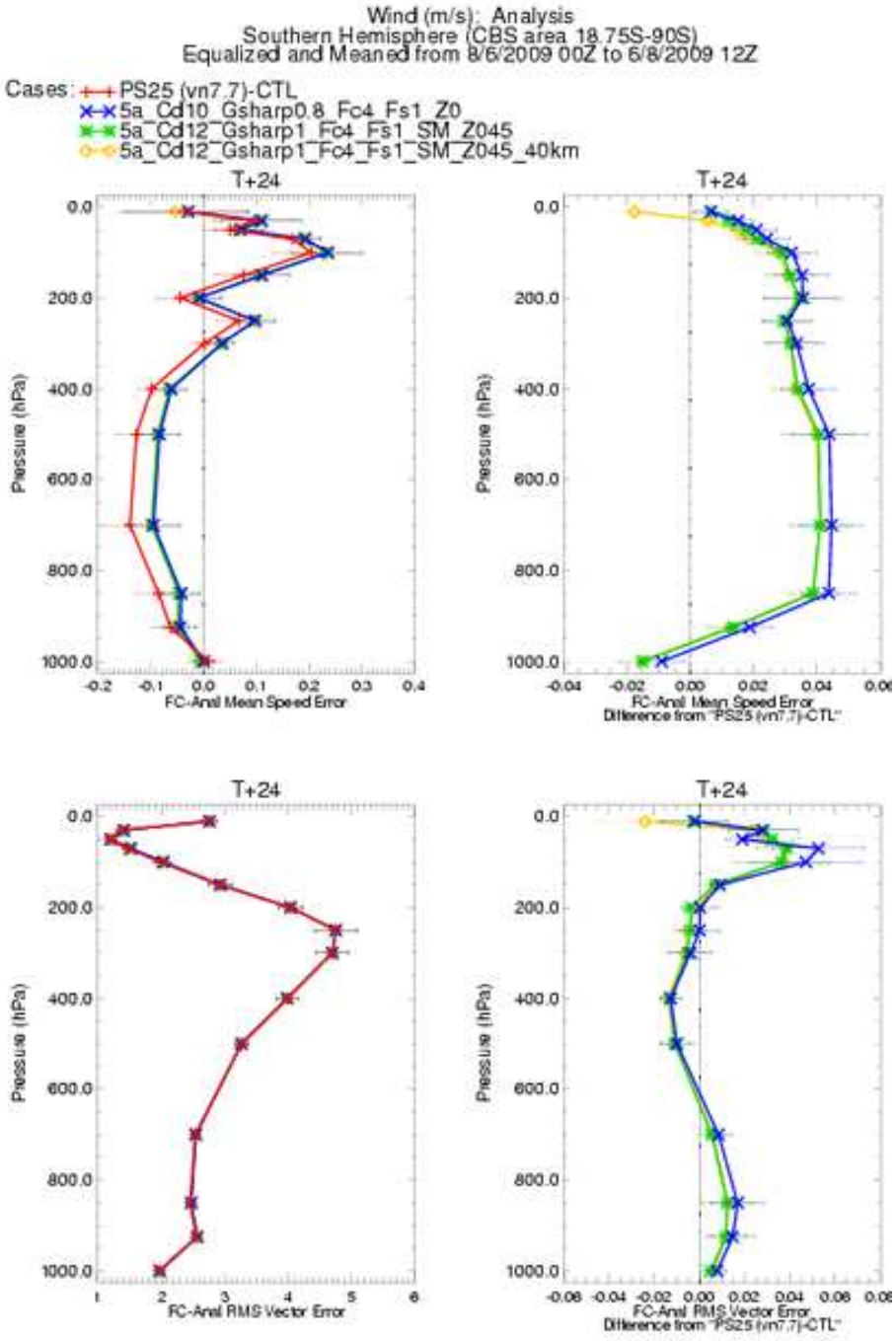

Figure 19: Forecasts (at T+24) compared to analyses for profiles of wind speed in the Southern Hemisphere in Summer 2009.

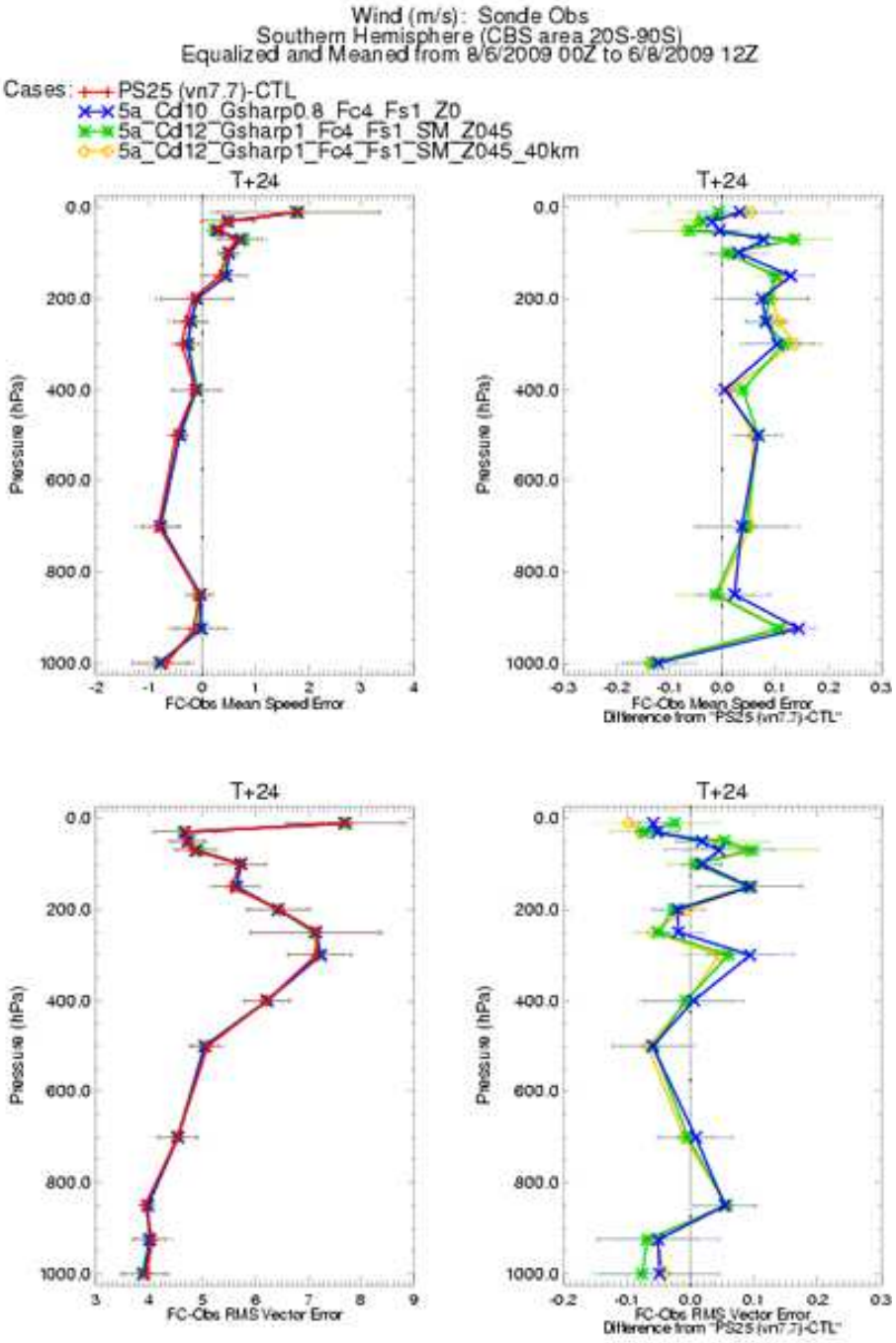

Figure 20: As Fig. 19 but comparison against sonde observations.

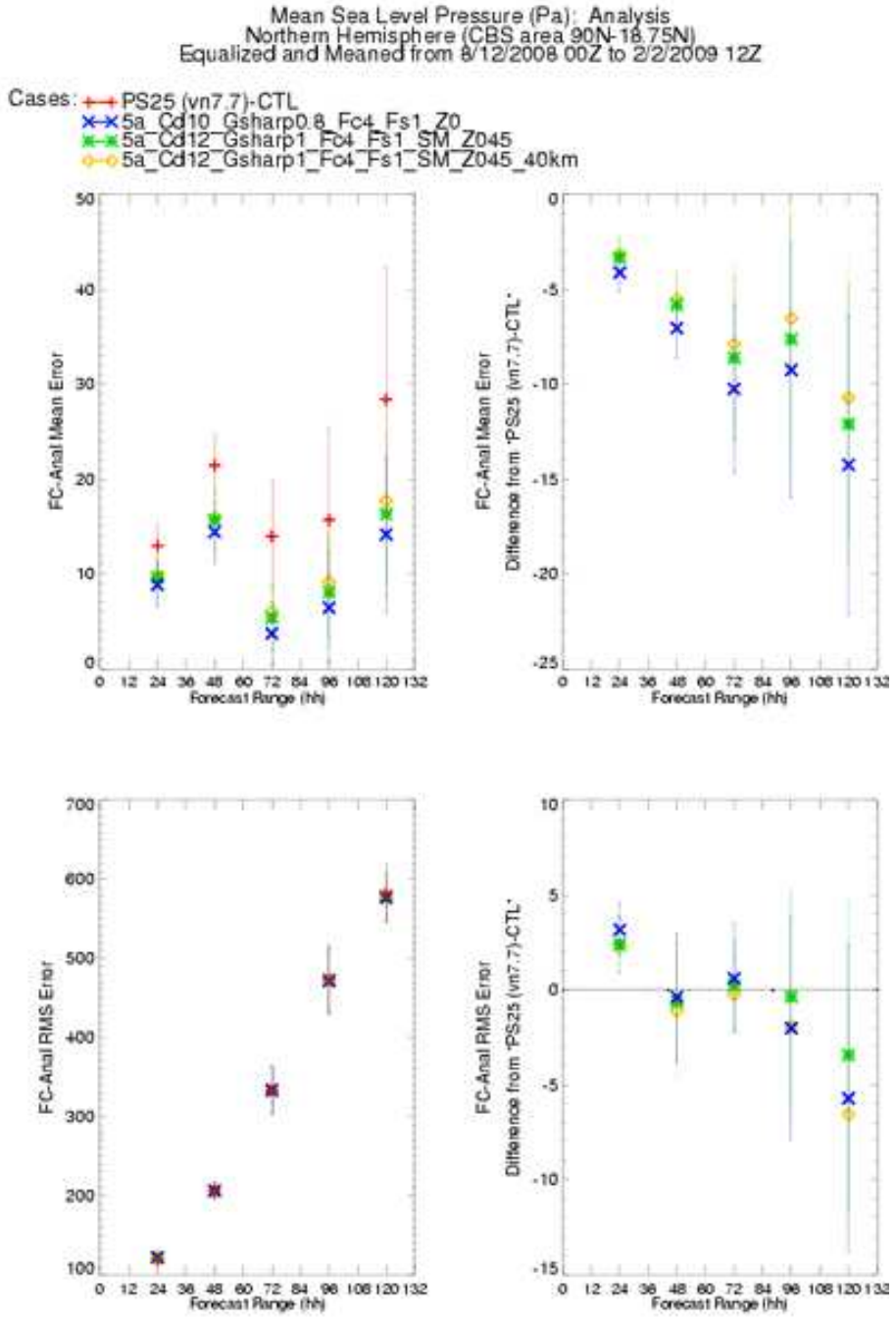

Figure 21: Forecasts compared to analyses for mean sea level pressure in the Northern Hemisphere in Winter 2008/2009

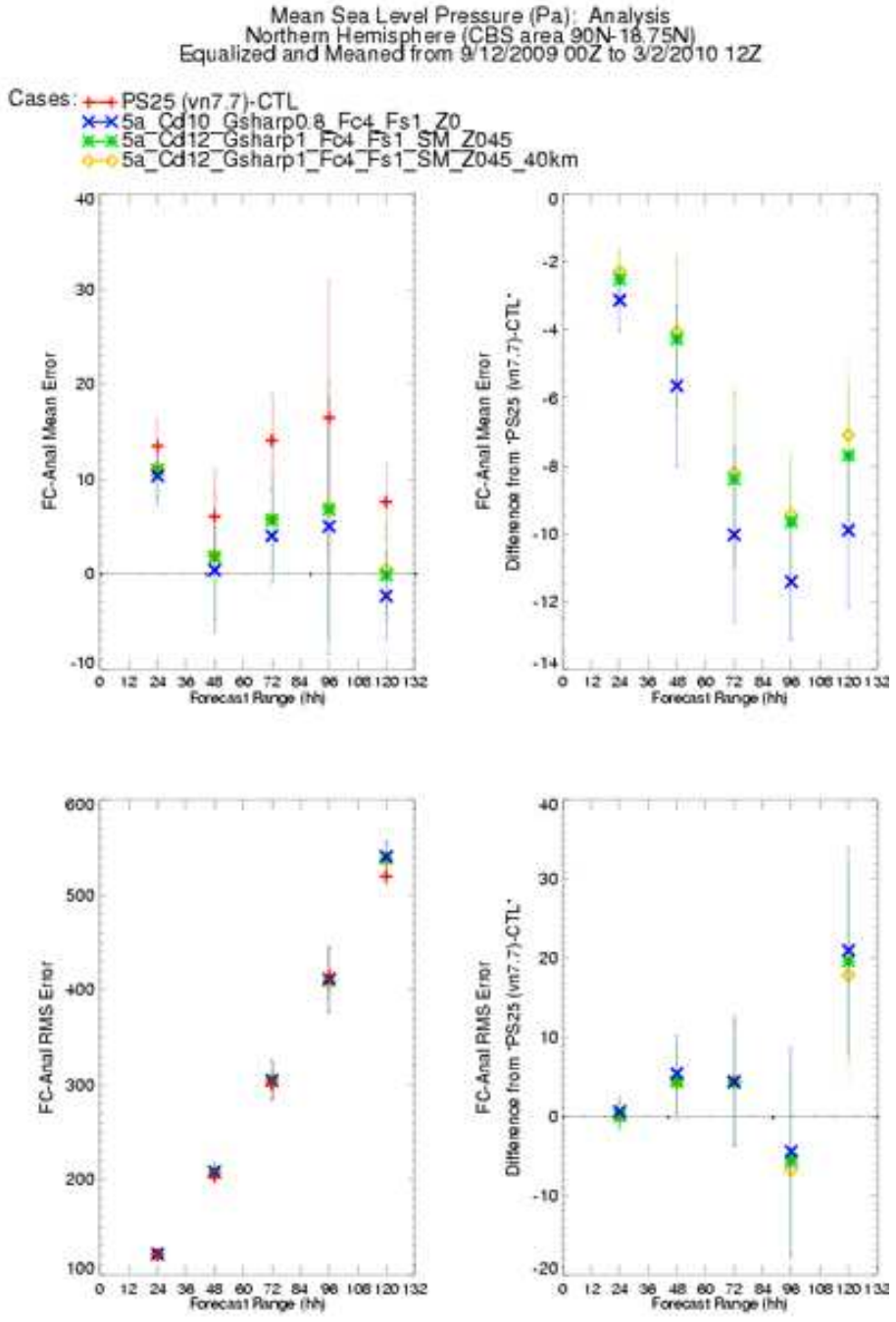

Figure 22: Forecasts compared to analyses for mean sea level pressure in the Northern Hemisphere in Winter 2009/2010

in the bias is less significant (bias reduced by approximately 1/8) and that the degradation in rms error is not robust. Figure 24 displays the results for winter 2009/2010. As with the comparison against analyses for winter 2008/2009 these results indicate a near halving of the bias between 850 hPa and 200 hPa, although they suggest a degradation in the bias at low levels, and a slight degradation in rms error (of $< 2\%$) around 850 hPa. Comparison against sonde observations also reveals a significant decrease in the bias between 850 hPa and 200 hPa (of approximately one third), although the degradation in the bias at low-levels and the degradation in rms error around 850 hPa is much less in evidence. In summary, in the northern hemisphere in winter the 5a scheme appears to perform at least as well as the CONTROL and displays some improvement in the bias in the wind speed between 850 hPa and 300 hPa.

Finally in the tropics there are only negligible changes in mean sea level pressure regardless of the season or comparator (i.e. observations or analyses) used (not shown). However, in all seasons a small degradation in bias and rms error is seen in the 850-800hPa winds when the comparison is done against the analyses. As an example, Fig. 25 shows forecasts at T+24 compared to analyses for profiles of wind speed in summer 2008. However, this signal is not generally present when the forecasts are compared against sonde observations (not shown) and so may not be robust.

In conclusion NWP case study tests of the 5a CONTROL set-up indicate near neutral performance when compared with the CONTROL, with some suggestion of improvements in bias in wind speed at T+24 between 850 hPa and 300 hPa at mid-high latitudes in the winter hemisphere and an improvement in bias in mean sea level pressure in the southern hemisphere in the austral winter. On the negative side, comparison against analyses indicates that the 850 hPa winds in the tropics may be worsened slightly. This could be a significant issue in terms of getting the new scheme into the operational model as tropical 850 hPa winds have a large impact on the NWP index. However, this signal is not generally present in the comparison against observations, suggesting that it is worth putting the 5a scheme into a VAR trial in order to assess it's performance in more detail.

5.2 More detailed comparison of 5a control with 4a control

In this section a more detailed comparison of the behaviour of the 5a CONTROL with the (4a) CONTROL will be carried out, using operational analysis data where available. We will focus on the winter (DJF) case studies (10 cases) in the first day of the forecast and average the data over these 10 cases in order to obtain more robust results. Note that the surface stress from the orographic drag scheme will not be shown in this report due to a bug in this diagnostic in the 5a CONTROL (which has since been corrected).

Figure 26 shows the mean sea level pressure averaged over all winter case study forecasts at T+24. In some regions the 5a CONTROL slightly alleviates the errors seen in the CONTROL (e.g. over Antarctica) whereas in other regions the errors are slightly worsened (e.g. the Himalayas and the Rockies). However, differences are generally small as implied by the verification results seen in

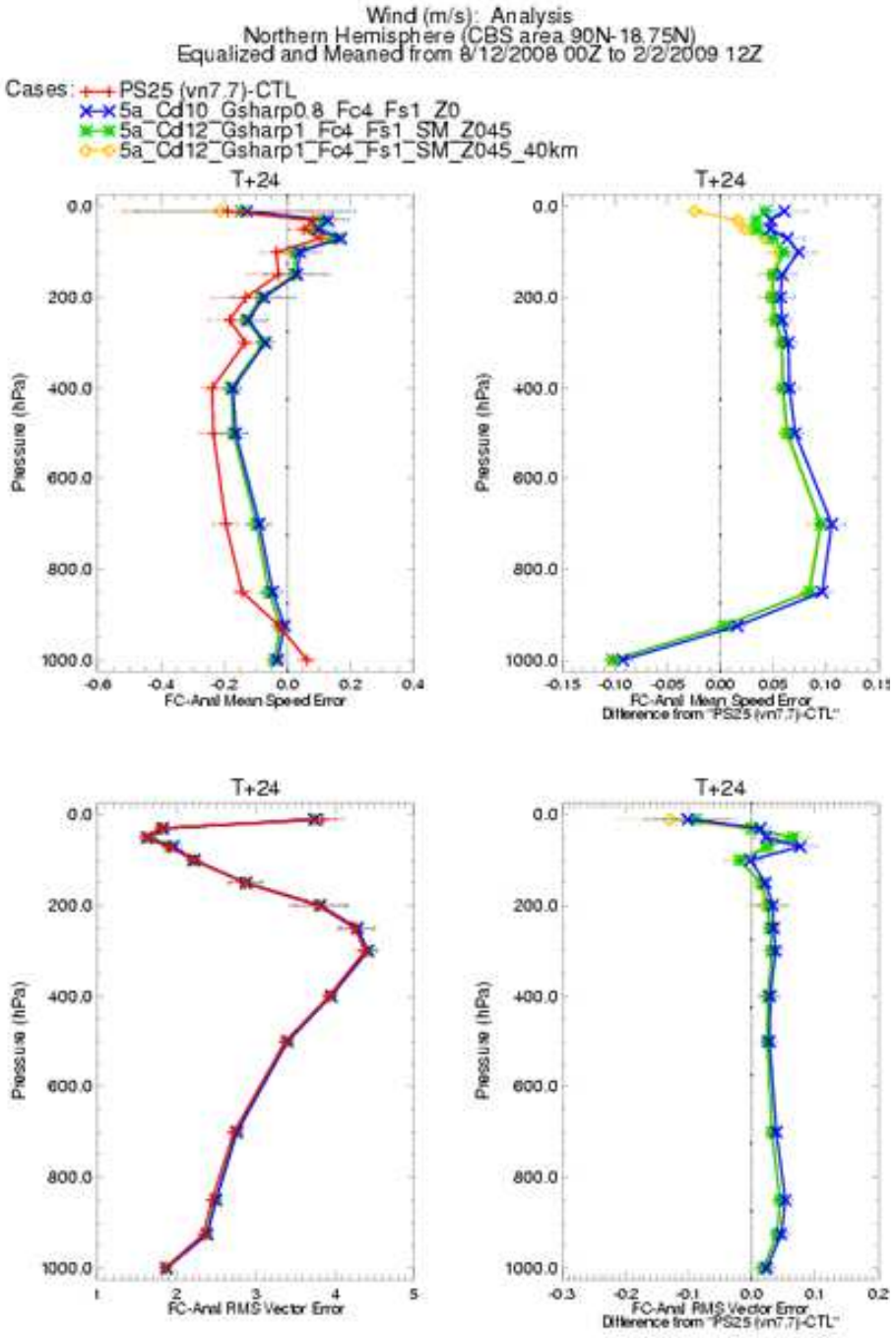

Figure 23: Forecasts (at T+24) compared to analyses for profiles of wind speed in the Northern Hemisphere in Winter 2008/2009

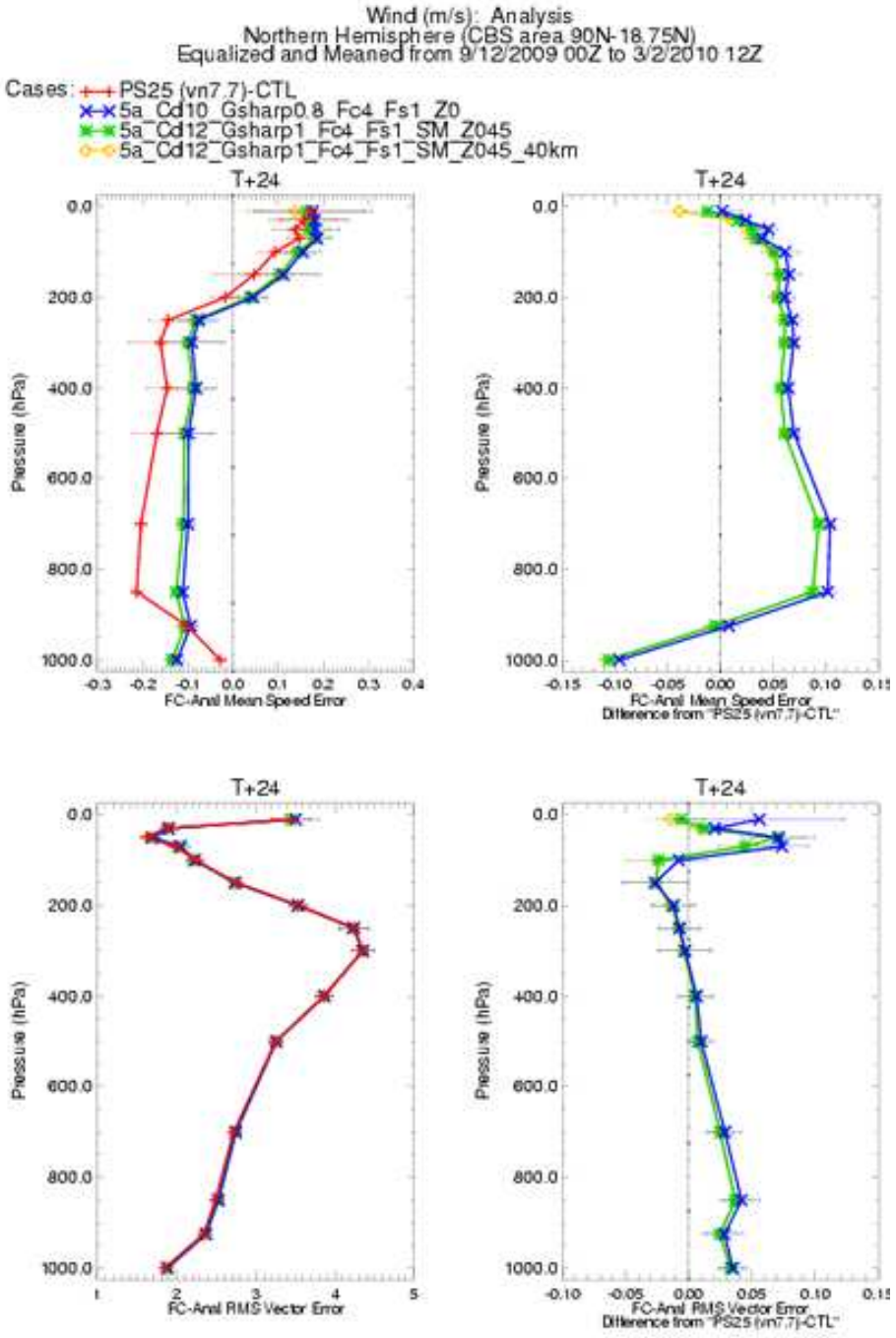

Figure 24: Forecasts (at T+24) compared to analyses for profiles of wind speed in the Northern Hemisphere in Winter 2009/2010

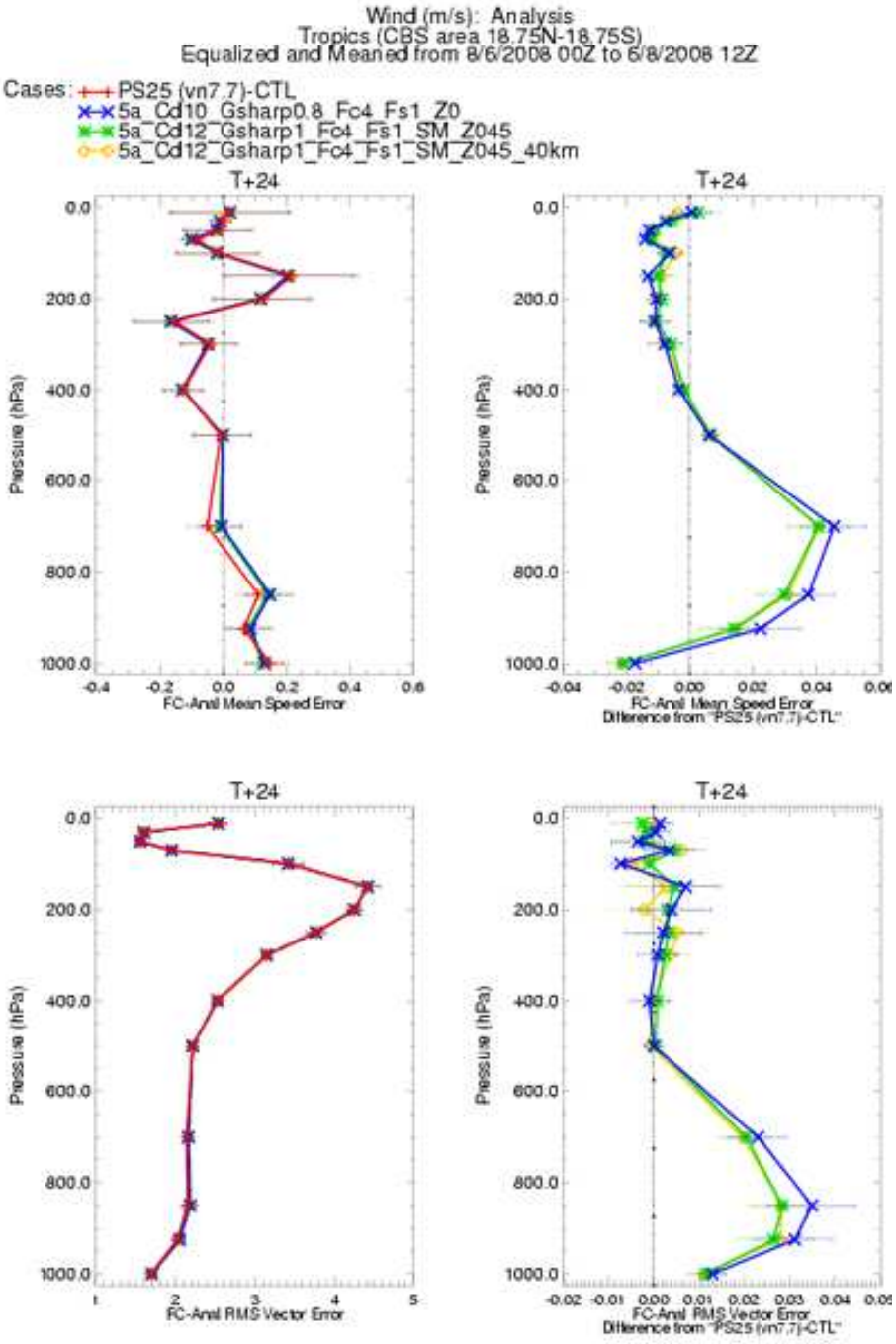

Figure 25: Forecasts (at T+24) compared to analyses for profiles of wind speed in the Tropics in Summer 2008

Figs. 21 and 22. As a brief aside it is worth noting that when Fig. 26 was repeated for all summer (JJA) cases (Fig. 27) a worrying looking signal was evident over Antarctica (near 160° E). As yet it has not been possible to ascertain the reason for this signal but this will be the subject of further analysis.

Figure 28 shows the zonal wind at 850hPa, one would expect differences in the wind at this height to dominated by differences in flow blocking drag. Figure 28 reveals that at a height of 850 hPa the differences between the 5a CONTROL and CONTROL are generally small (as would be expected from the small differences in errors seen in section 5.1). However for some locations, most notably the southern Andes region, the difference between the 5a CONTROL and CONTROL is of a similar size to the difference between the CONTROL and the analysis. In the southern Andes region the 5a CONTROL generally increases the error with respect to the analysis. In contrast, over the Himalayas errors are reduced in the 5a CONTROL. It is not clear from Fig. 28 where the increased bias and rms error seen in the tropical (18.75°N-18.75°S) winds around 850 hPa (Fig. 25) comes from.

Figure 29 shows the average zonal wind increment applied by the orographic drag scheme over the lowest 3 km of the atmosphere. The average zonal wind increment over the Himalayas is significantly smaller in the 5a CONTROL than in the CONTROL, indicative of less effective flow blocking in the 5a CONTROL than the CONTROL. Significantly weaker blocking in the 5a CONTROL is also observed over the southern Andes (note, the effect is masked in Fig. 29 due to a lack of other significant topography at that latitude). In contrast, more blocking drag is parametrized by the 5a CONTROL near the south pole. Figure 30 shows the average zonal wind increment applied by the boundary layer scheme. It is clear from comparison of Fig. 29(bottom) with Fig. 30(bottom) that the boundary layer scheme generally counteracts the differences seen in the orographic drag. This explains how the orographic drag can be so different in the 5a CONTROL without significant errors being seen in the verification results (in section 5.1).

Figure 31 shows the average zonal wind at 70 hPa compared to the analysis data. At a height of 70 hPa significant differences between the 5a CONTROL and the CONTROL are seen over the Himalayas, the southern Andes and the southern Rockies which generally indicate increased errors in the 5a CONTROL in these regions. Figure 32 shows the zonally averaged zonal wind increment from the orographic gravity wave drag scheme. Figure 32 reveals significant differences in the northern hemisphere stratosphere which are indicative of weaker stratospheric gravity wave drag in the 5a CONTROL than in the CONTROL. Note that the drag over the southern Andes is again deceptively small when displayed in this way, since the results have been averaged around a latitude band with very little significant topography. The differences in stratospheric drag between 5a CONTROL and CONTROL indicate that an increase in the gravity wave amplitude factor, G, may lead to better results. Note that Fig. 32 also indicates differences in gravity wave drag close to the surface, this difference may be a result of a bug in the 4a scheme which means that gravity waves are saturated at launch (which will lead to increased low-level breaking in the CONTROL), this has

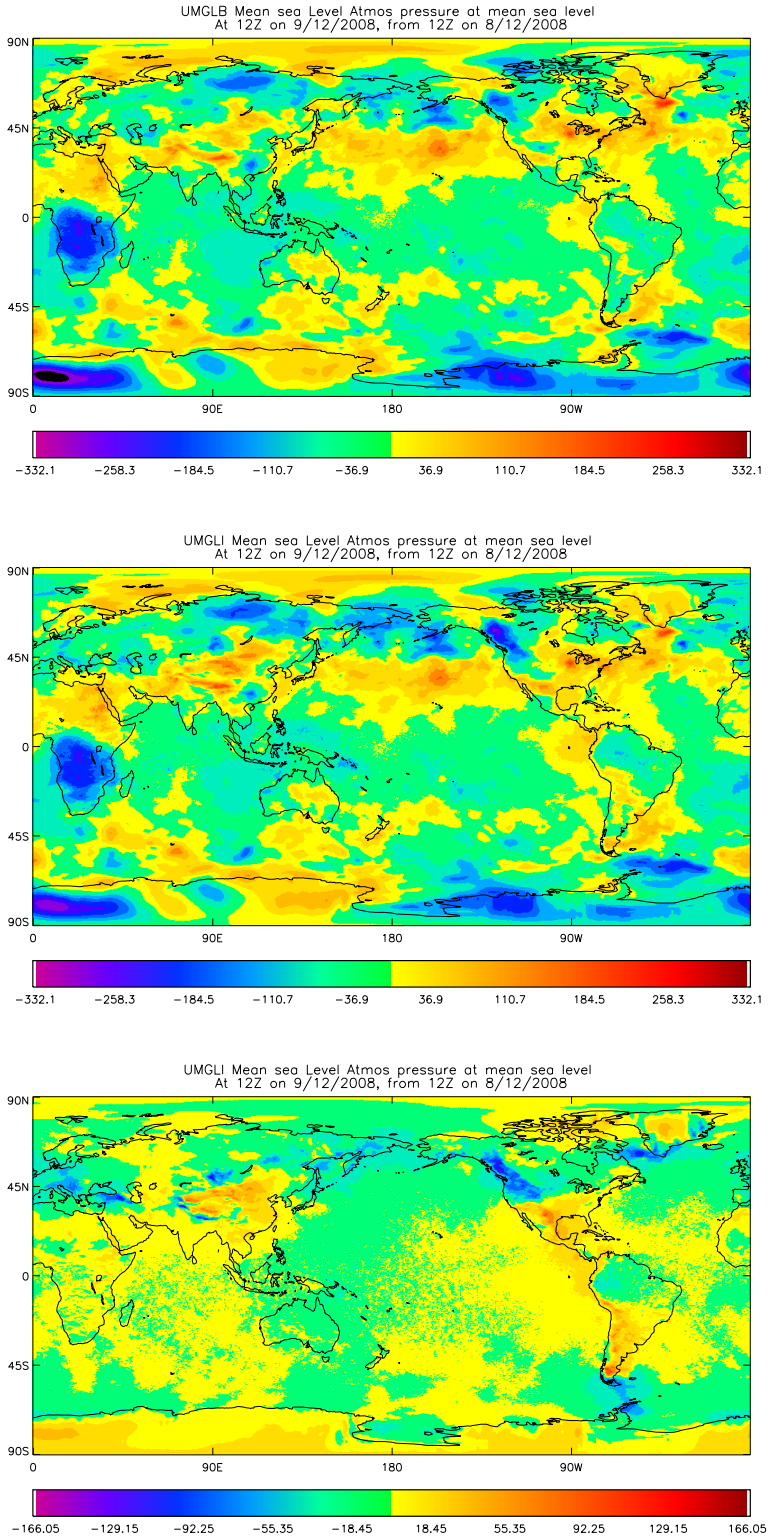

Figure 26: Average mean sea level pressure for all winter (DJF) case study forecasts at T+24 for: (top) CONTROL - ANALYSIS; (middle) 5a CONTROL - ANALYSIS; and (bottom) 5a CONTROL - CONTROL (note the contour interval is half of that for the two other plots).

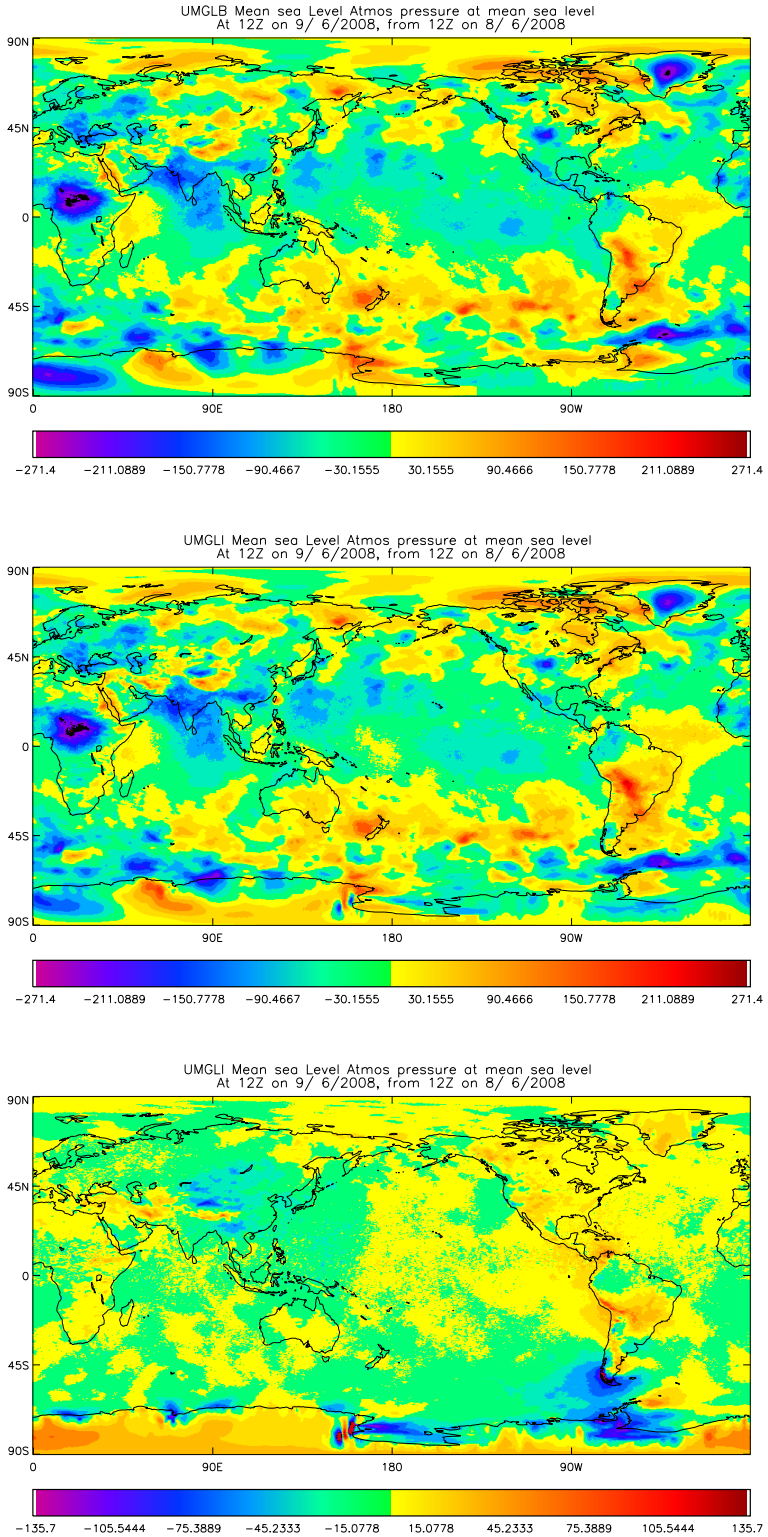

Figure 27: As Fig. 26 but for all summer (JJA) case study forecasts.

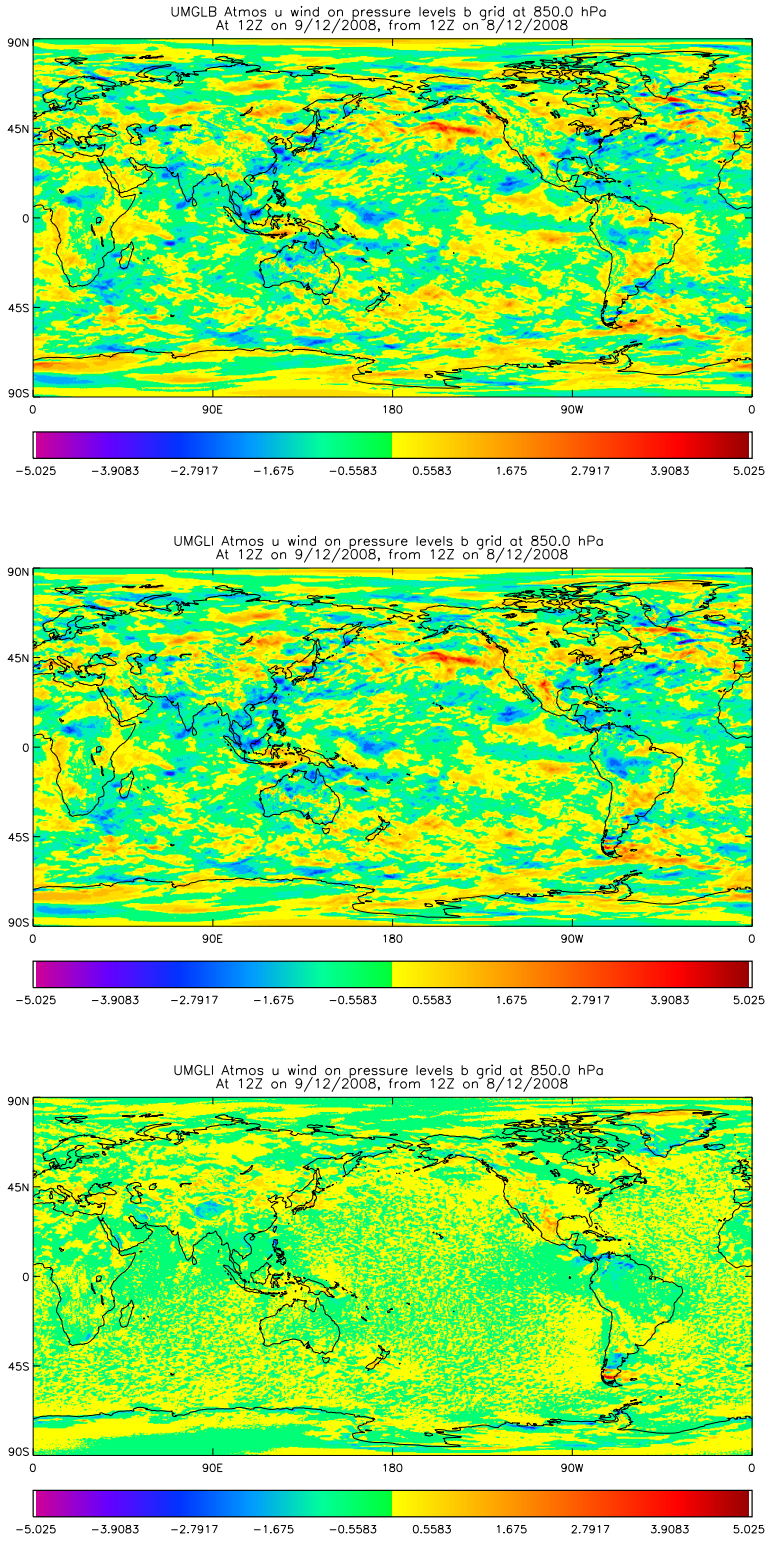

Figure 28: Average zonal wind at 850 hPa for all winter (DJF) case study forecasts at T+24 for: (top) CONTROL - ANALYSIS; (middle) 5a CONTROL - ANALYSIS; and (bottom) 5a CONTROL - CONTROL.

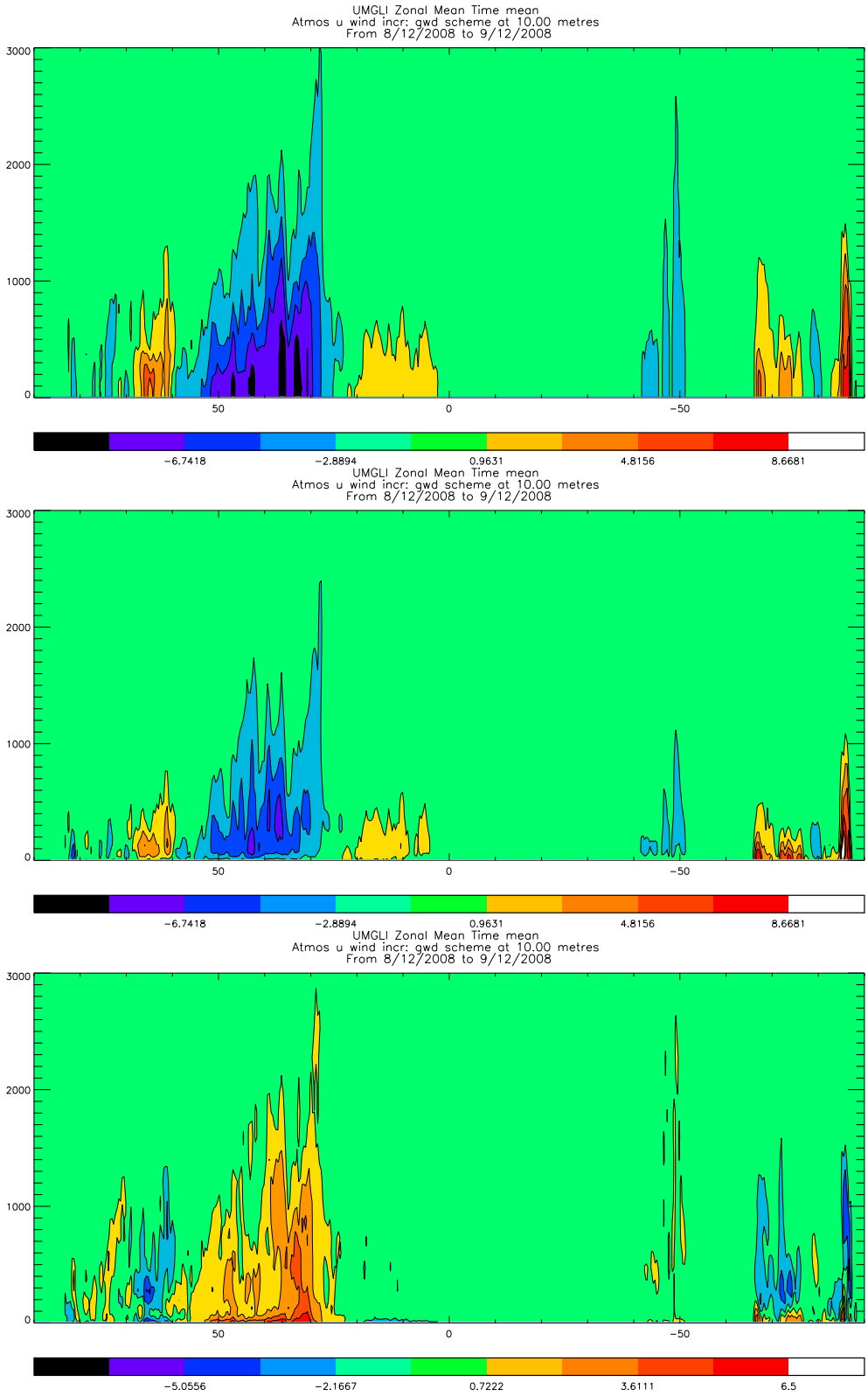

Figure 29: Zonally averaged zonal wind increment from the orographic drag scheme over all winter (DJF) case study forecasts (increments accumulated over the first 24 hours of the forecast) for: (top) CONTROL; (middle) 5a CONTROL; and (bottom) 5a CONTROL - CONTROL.

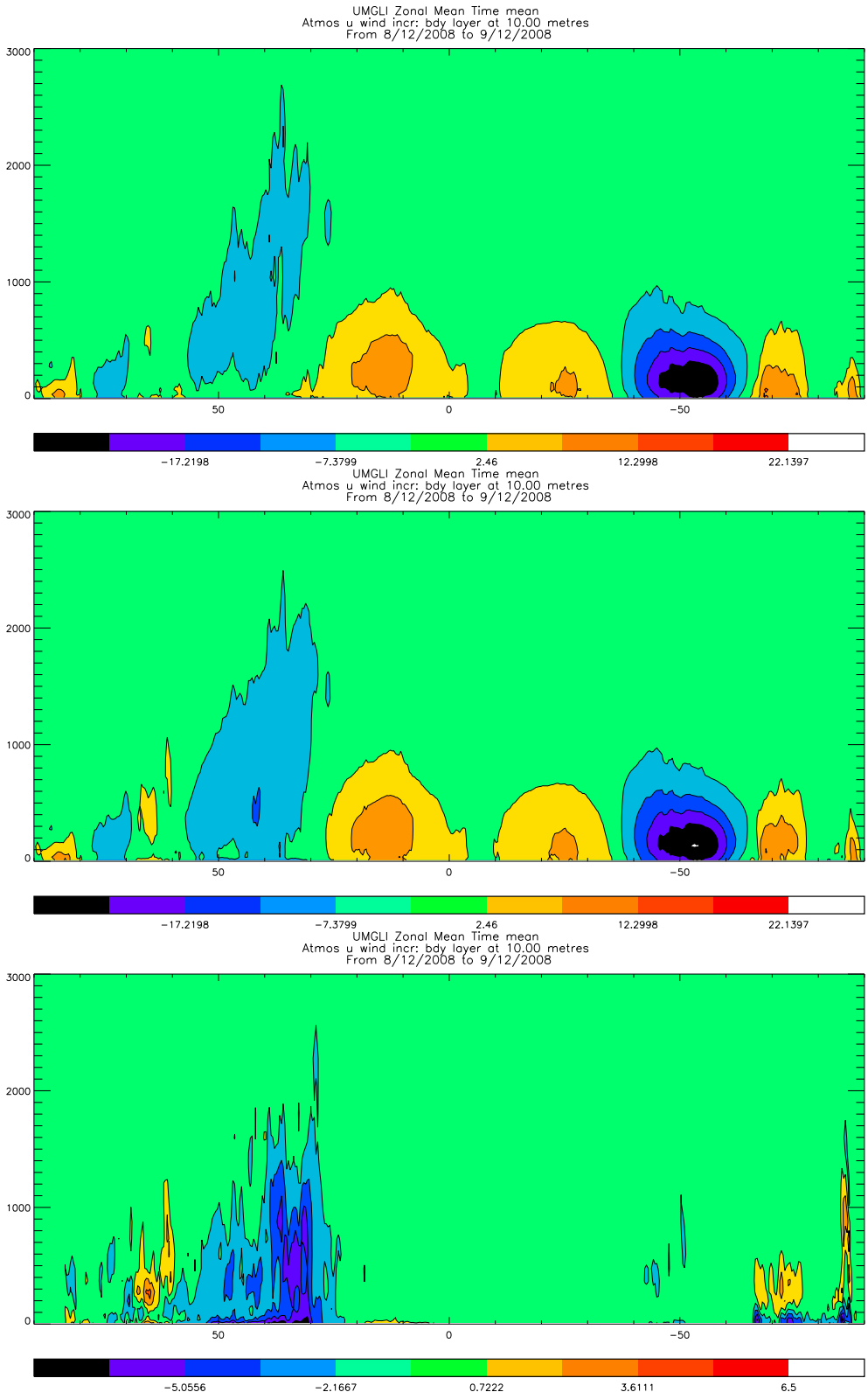

Figure 30: Zonally averaged zonal wind increment from the boundary layer scheme over all winter (DJF) case study forecasts (increments accumulated over the first 24 hours of the forecast) for: (top) CONTROL; (middle) 5a CONTROL; and (bottom) 5a CONTROL - CONTROL (note the contour interval for this plot is the same as that for Fig. 29 bottom plot).

been fixed in the 5a scheme.

In summary, it appears that the performance of the 5a CONTROL is competitive with the CONTROL (supporting the verification results seen in the previous section). However, the 5a CONTROL has weaker gravity wave activity than the control which suggests that the gravity wave amplitude factor, G, may need to increased to fully optimise the scheme.

5.3 Verification against observations and analyses: Alternative set-ups for 5a scheme

Here we consider briefly the performance of various alternative set-ups for the 5a scheme for which case study suites have been run: 5a SMOOTH; 5a GWD TO LID; 5a ALT SSO; and 5a BLOCK. Note that these tests were mistakingly run with 40 km filtering for the SSO however this does not affect the conclusions drawn in this section.

- 5a SMOOTH (as 5a CONTROL but smoothing ($\chi = 1$) and $G = 1$, $Cd = 12$)

  The plots shown in section 5.1 revealed that 5a SMOOTH performs in a similar way to 5a CONTROL.

- 5a GWD TO LID (as 5a SMOOTH but apply orographic gravity wave drag above $z = 40$ km)

  In the current operational model no orographic gravity wave drag is applied above $z = 40$ km since when the model lid was raised to $z = 80$ km large accelerations were being applied near the top of the model which led to wind reversals and numerical instability. For example at a height of 0.1 hPa differences in the zonal wind of up to 130 ms^{-1} were seen at T+120 between a control run without gravity wave drag above 40km and a run with gravity wave drag throughout the depth of the model. The 5a GWD TO LID test was done in order to assess whether the introduction of smoothing the gravity wave drag would prevent these zonal wind reversals and make the model more stable. Encouragingly no model stability problems were experienced with this set-up and all 20 forecasts run successfully (note: it was suggested that the CONTROL (4A) model would fall over 3 or 4 times whilst running a case study suite with gravity wave drag on above 40 km (Stuart Webster, personal communication)). However, very large differences in the zonal wind at 0.1 hPa were seen in individual forecasts at T+120. The largest difference (5a GWD TO LID-CONTROL) was -122 ms^{-1} and six forecasts contained differences of greater than 100 ms^{-1}. An example of this behaviour is shown in Fig. 33. These zonal wind reversals suggest that the introduction of smoothing the drag is insufficient to prevent numerical stability problems if gravity wave drag is applied above 40 km. Therefore it is currently recommended that gravity wave drag be switched off above 40 km in the recommended set-up for the 5a scheme. It may be possible to resolve this issue in future by adjusting F_{sat} and χ.

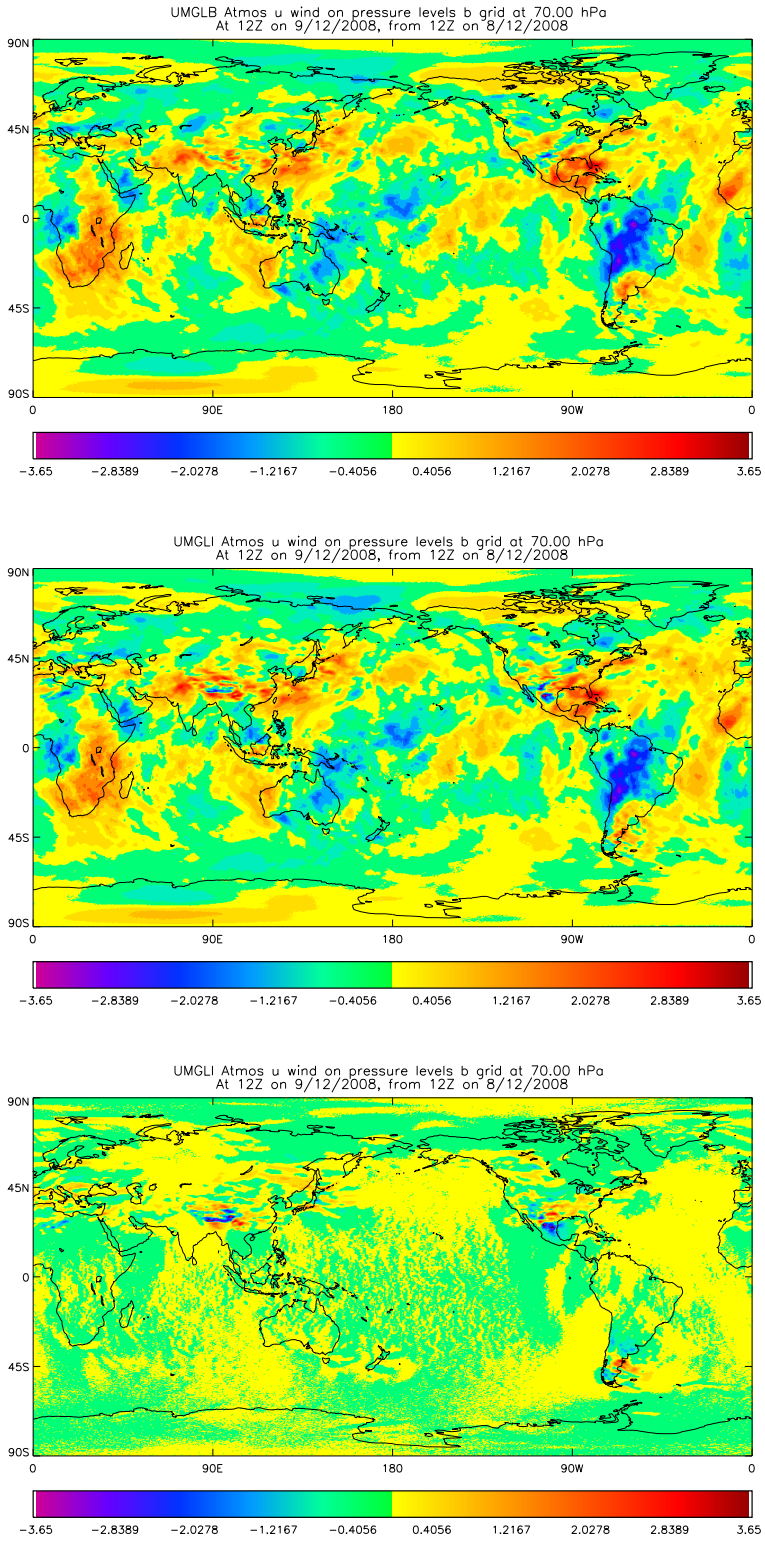

Figure 31: Average zonal wind at 70 hPa for all winter (DJF) case study forecasts at T+24 for: (top) CONTROL - ANALYSIS; (middle) 5a CONTROL - ANALYSIS; and (bottom) 5a CONTROL - CONTROL (note that the contour interval for this plot is one tenth of that for the (top) and (middle) plots.

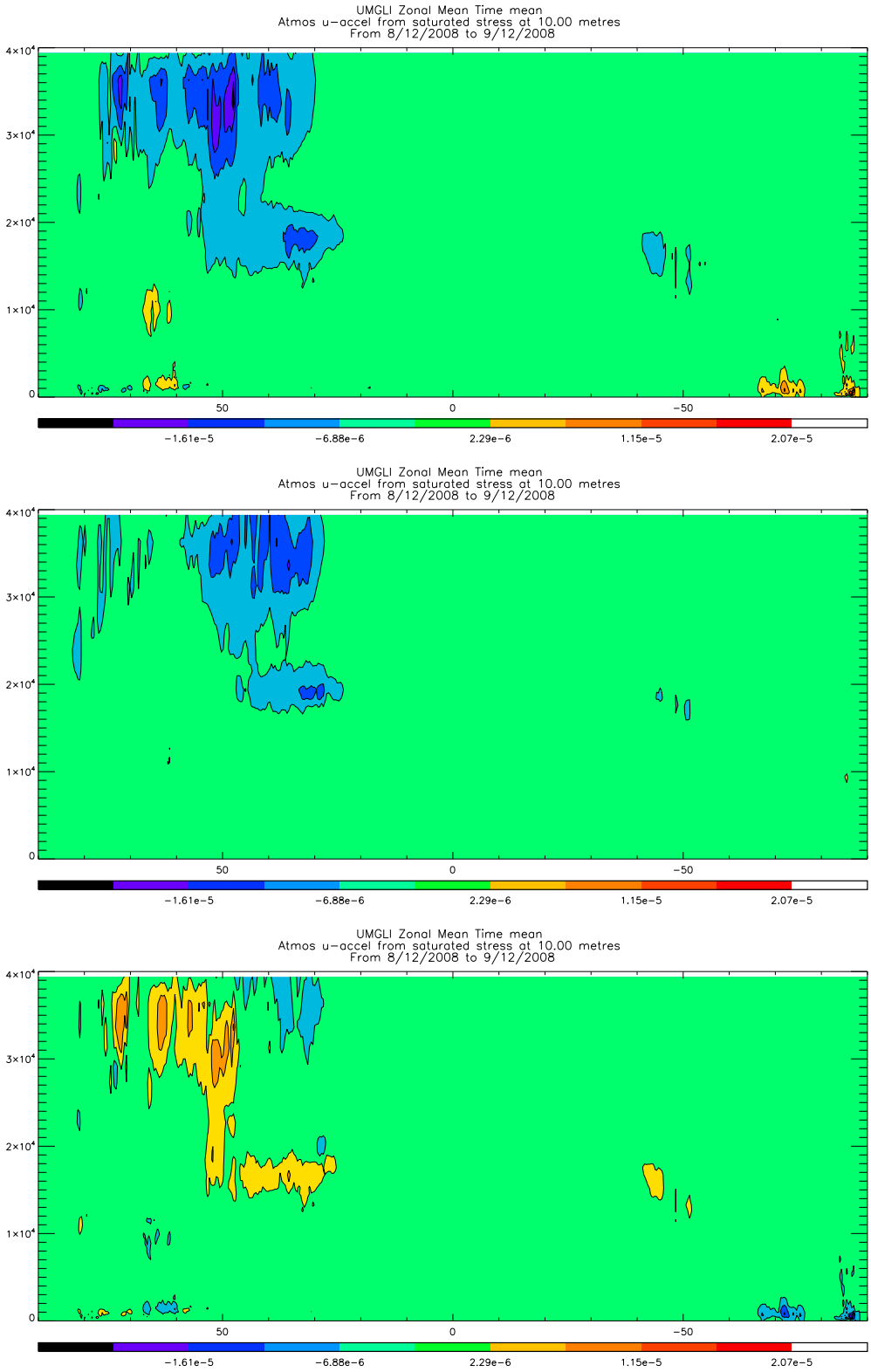

Figure 32: Zonally averaged zonal wind increment from orographic gravity wave drag averaged over all winter (DJF) case study forecasts (increments averaged over the first 24 hours of the forecast) for (top) CONTROL (middle) 5a CONTROL and (bottom) 5a CONTROL - CONTROL

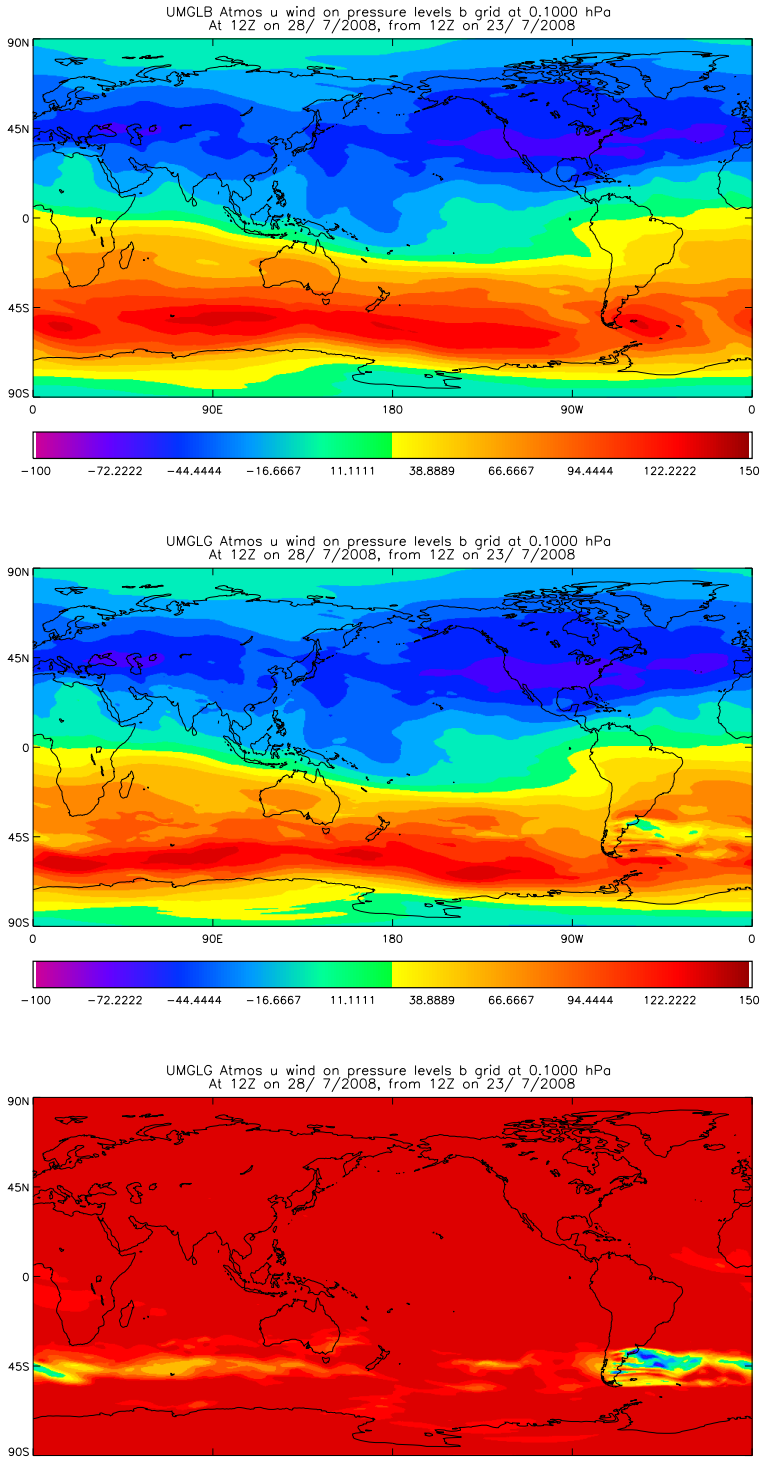

Figure 33: Zonal wind at 0.1 hPa at T+120 for (top) CONTROL (middle) 5a GWD TO LID and (bottom) 5a GWD TO LID - CONTROL

- 5a ALT SSO (as 5a SMOOTH except alternative SSO definitions used (no σ_{ij}, anisotropy, $\gamma = 1$; orientation, $\Psi = 0$; and slope, $\alpha = H/(0.25\Delta x)$

  The case study forecasts with 5a ALT SSO appear encouraging. The errors (against observations and analyses) are larger for 5a ALT SSO than for the 5a CONTROL but I believe that they could be reduced to an acceptable level with further tuning (e.g. of Cd and G). However, one issue that arises with 5a ALT SSO is a significant increase in the error near the poles (especially in the winter hemisphere). As an example of this error, Fig. 34 shows the mean sea level pressure for all summer (JJA) forecasts at T+24 for both the CONTROL and 5a ALT SSO. Significant errors are apparent over Antarctica which are due to much larger values of the slope parameter, α, in this region (seen in Fig. 9) due to the dependency of slope on the zonal width of the grid-box, Δx, which reduces significantly near the poles. It may be possible to overcome this issue by introducing a minimum Δx (which could be a fraction of the maximum Δx at that model resolution) or by replacing Δx with Δy in the definition of α.

- 5a BLOCK (as 5a SMOOTH but $Z_b = H$ for flow blocking (normal Z_b used for cut-off mountain calculation for gravity wave drag))

This is one possible way of increasing the amount of flow blocking drag in the 5a scheme (and may allow us to move away from using such a large value of F_c in the longer term, refer back to section 4.2 for more details). Whilst the errors (against observations and analyses) are larger for 5a BLOCK than for the 5a CONTROL I believe that they could be reduced to an acceptable level with further tuning. However, 5a BLOCK was not stable in the case study suite, with one forecast falling over due to a model error (a result of not setting $l(z)$, a function of the anisotropy, to zero for all points). This bug can easily be corrected, and this option could be pursued further if appropriate.

6 Performance summary

In terms of computational cost the case study tests indicate that the new scheme (5a CONTROL) requires more CPU time than the current scheme (CONTROL). The case study tests were run on 4×32 processors for 615 time steps and indicate an increase in CPU time of $\approx 1 - 2\%$. One would hope that this can be decreased by optimising the code further (as only limited code optimisation has taken place to date) or possibly by running the parametrization less frequently than every time-step. There is no significant change in the memory usage.

Based on the N320L70 tests documented in this report the current recommended set-up for the 5a scheme is as follows: 6km filtering for sub-grid scale orography, $Cd = 10$, $G = 1$, $Z0_{eff} = 0.45$, Smoothing on ($\chi = 1$). The next stage of testing will be to run a VAR trial at N320L70 for 1 week in the northern hemisphere winter (DJF) with this configuration. If this set-up is not competitive then the tests indicate that it could be made more similar to the control, if G was increased. Once we

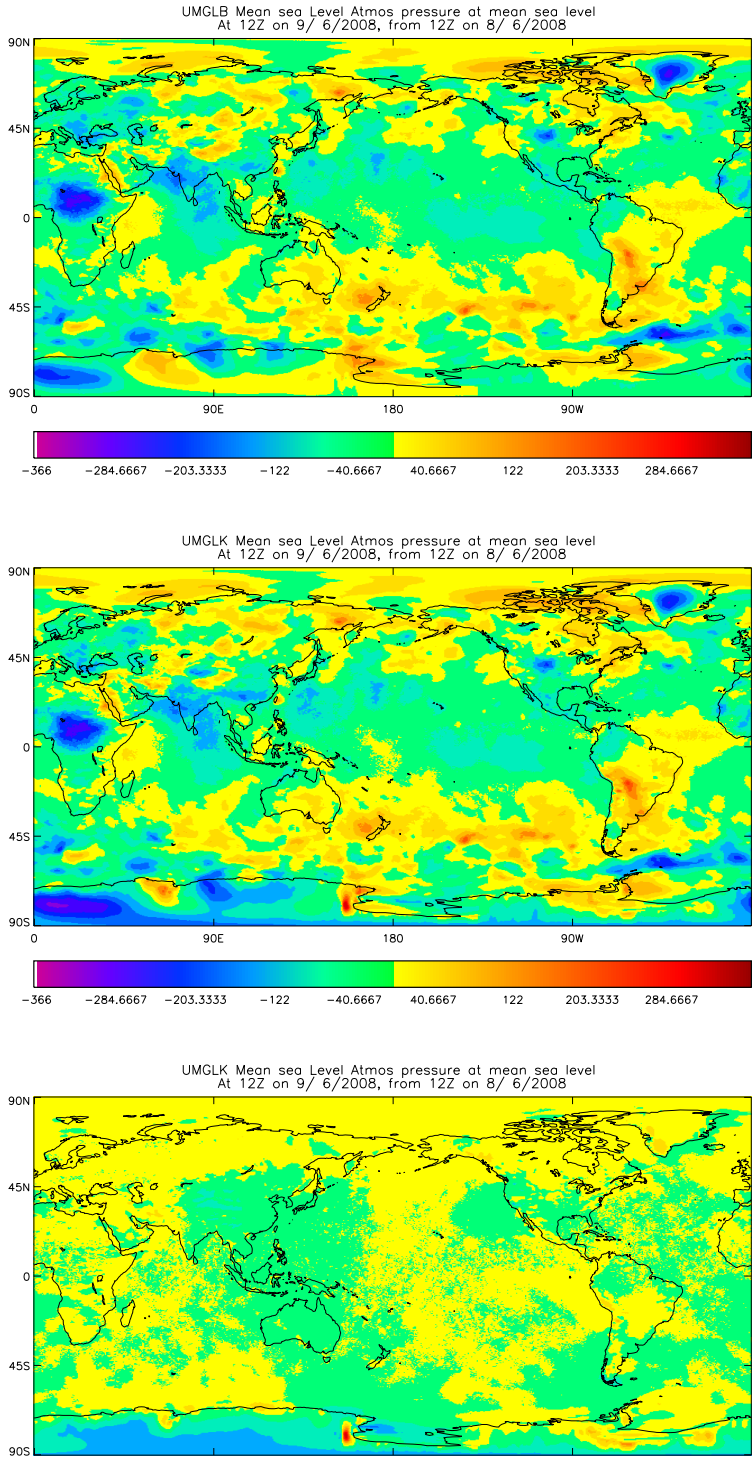

Figure 34: Average mean sea level pressure for all summer (JJA) case study forecasts at T+24 for: (top) CONTROL - ANALYSIS; (middle) 5a ALT SSO - ANALYSIS; and (bottom) 5a ALT SSO - CONTROL.

have converged on a good set-up (which produces good results in a VAR trial) this set-up will be used to run N512 case study tests and to produce a climate validation note.

In terms of the alternative set-ups both 5a GWD TO LID and 5a BLOCK could be pursued further with some more tuning tests and a small bug fix to the 5a BLOCK code. The more adventurous option of 5a ALT SSO could also be taken further, either in it's current form or as a variant where the alternative SSO is only used for the flow blocking scheme. The work required would involve some further tuning and a slight change to the formulation of the slope parameter (to prevent large values in polar regions).

7 Summary

This report has described the formulation and testing of a new mountain drag scheme for the MetUM called the 5a scheme. The scheme has been developed in order to improve the physical basis of orographic drag parametrization in the MetUM and to introduce more flexibility by allowing the amplitude of the flow blocking and gravity wave response to be determined separately (rather than being defined by a single parameter). It was hoped that the introduction of a new scheme would also allow us to move away from several unphysical settings that are used by the current scheme namely: a critical Froude number of 4, switching off gravity wave drag above 40km for model stability and defining the sub-grid scale orography (SSO) using non-convergent and noisy parameters (σ_{ij}). Unfortunately tests revealed that at present the 5a scheme is unlikely to allow us to re-tune the critical Froude number or apply gravity wave drag throughout the depth of the model. However, tests where an alternative formulation of the SSO was used were more positive, implying that it may be possible to move away from using the non-convergent parameters (σ_{ij}).

Assessment of the 5a scheme using case study tests revealed that it's performance was generally neutral when compared to the current scheme. However, the current recommended set-up appears to degrade the tropical winds at 850 hPa when compared to the analysis (increasing the rms error by $\approx 1\%$), although this signal is not seen when the results are compared to observations. If this signal is also seen in a VAR trial then some re-tuning could be necessary in order to achieve competitive performance with the current scheme. The tests done for a single forecast (detailed in section 4) give useful guidance regarding the sensitivity to various parameters in order to aid efficient re-tuning of the scheme.

References

[Brown, 2005] Brown, A. R. (2005). Tests of modifications to the lott and miller orographic parametrization.

[Epifanio and Qian, 2008] Epifanio, C. C. and Qian, T. (2008). Wave-turbulence interactions in a breaking mountain wave. *J. Atmos. Sci.*, 65:3139–3158.

[Gregory et al., 1998] Gregory, D., Shutts, G. J., and Mitchell, J. R. (1998). A new gravity-wave drag scheme incorporating anisotropic orography and low-level wave breaking: Impact on the climate of the UK Meteorological Office Unified Model. *Q. J. R. Meteorol. Soc.*, 124:463–493.

[Lindzen, 1981] Lindzen, R. S. (1981). Turbulence and stress owing to gravity wave and tidal breakdown. *J. Geophys. Res.*, 86:9707–9714.

[Lott and Miller, 1997] Lott, F. and Miller, M. J. (1997). A new subgrid-scale orographic drag parametrization: Its formulation and testing. *Q. J. R. Meteorol. Soc.*, 123:101–127.

[McFarlane, 1987] McFarlane, N. A. (1987). The effect of orographically excited gravity wave drag on the general circulation of the lower stratosphere and troposphere. *J. Atmos. Sci.*, 44:1175–1800.

[Phillips, 1984] Phillips, D. S. (1984). Analytical surface pressure and drag for linear hydrostatic flow over three-dimensional elliptical mountains. *J. Atmos. Sci.*, 41:1073–1084.

[Scinocca and McFarlane, 2000] Scinocca, J. F. and McFarlane, N. A. (2000). The parametrization of drag induced by stratified flow over anisotropic orography. *Q. J. R. Meteorol. Soc.*, 126:2353–2393.

[Shutts and Vosper, 2011] Shutts, G. and Vosper, S. B. (2011). Stratospheric gravity waves revealed in NWP model forecasts. *Q. J. R. Meteorol. Soc.*, 137:303–317.

[Vosper et al., 2009] Vosper, S. B., Wells, H., and Brown, A. R. (2009). Accounting for non-uniform static stability in orographic drag parametrization. *Q. J. R. Meteorol. Soc.*, 135:815–822.

[Wallace et al., 1983] Wallace, J. M., Tibaldi, S., and Simmons, A. J. (1983). Reduction of systematic forecast errors in the ECMWF model through the introduction of an envelope orography. *Q. J. R. Meteorol. Soc.*, 109:683–717.

[Webster et al., 2003] Webster, S., Brown, A. R., Cameron, D. R., and Jones, C. P. (2003). Improvements to the representation of orography in the Met Office Unified Model. *Q. J. R. Meteorol. Soc.*, 129:1989–2010.

Met Office
FitzRoy Road, Exeter
Devon, EX1 3PB
UK

Tel: 0370 900 0100
Fax: 0370 900 5050
enquiries@metoffice.gov.uk
www.metoffice.gov.uk

Produced with the Met Office LaTeX template v2.0.0